DAHLGREN DIVISION
NAVAL SURFACE WARFARE CENTER
Dahlgren, Virginia 22448-5100

NSWCDD/TR-96/46

ABSOLUTE ALIGNMENT OF SENSORS

BY RONALD E. HELMICK JEFFREY E. CONTE THEODORE R. RICE
SYSTEMS RESEARCH AND TECHNOLOGY DEPARTMENT

MAY 1996

REPORT DOCUMENTATION PAGE

Form Approved
OMB No. 0704-0188

1. AGENCY USE ONLY (Leave blank)	2. REPORT DATE	3. REPORT TYPE AND DATES COVERED
	May 1996	Final

4. TITLE AND SUBTITLE

Absolute Alignment of Sensors

5. FUNDING NUMBERS

6. AUTHOR(s)

Ronald E. Helmick, Jeffrey E. Conte, Theodore R. Rice

7. PERFORMING ORGANIZATION NAME(S) AND ADDRESS(ES)

Commander
Naval Surface Warfare Center
Dahlgren Division (Code B32)
17320 Dahlgren Road
Dahlgren, VA 22448-5100

8. PERFORMING ORGANIZATION REPORT NUMBER

NSWCDD/TR-96/46

9. SPONSORING/MONITORING AGENCY NAME(S) AND ADDRESS(ES)

10. SPONSORING/MONITORING AGENCY REPORT NUMBER

11. SUPPLEMENTARY NOTES

12a. DISTRIBUTION/AVAILABILITY STATEMENT

Approved for public release; distribution is unlimited.

12b. DISTRIBUTION CODE

13. ABSTRACT (Maximum 200 words)

Absolute alignment refers to the process of determining the true bias or offset errors in the data reported by a sensor. This report develops an algorithm for absolutely aligning the positional data reported by a tracking sensor using a target whose location is measured by the sensor and whose location can be precisely determined by some technique independently of the sensor's measurements. The algorithm also requires the location of the sensor to be precisely known. Any differences between the sensor-reported position of the target and the independently determined precise target location is attributed to bias errors in the track data reported by the sensor. These differences can be used to estimate the bias errors in the track data. A potential candidate for providing precise location information independently of the sensor's measurements is GPS (Global Positioning System). However, the algorithm is applicable to any technique that provides precise location information independently of the sensor's measurements. Simulation results are presented to illustrate the performance of the absolute alignment algorithm developed in this report.

14. SUBJECT TERMS

absolute alignment, modeled bias errors, true and sensor-reported positions, linear alignment model, nonlinear alignment model, bias estimation module, bias correction module

15. NUMBER OF PAGES

16. PRICE CODE

17. SECURITY CLASSIFICATION OF REPORTS	18. SECURITY CLASSIFICATION OF THIS PAGE	19. SECURITY CLASSIFICATION OF ABSTRACT	20. LIMITATION OF ABSTRACT
UNCLASSIFIED	UNCLASSIFIED	UNCLASSIFIED	UL

FOREWORD

The alignment algorithms and analysis discussed in this report were developed by the Digital Systems Branch (B32) of the Combat Systems Technology Group (B30). This effort was sponsored by the Amphibious Warfare Directorate Marine Corps Systems Command under the Marine Corps Exploratory Development Program, Marine Corps Landing Force Technical Program MQ1A (PE 62131 M), whose point of contact is R. L. Stiegler, Code G305, Naval Surface Warfare Center Dahlgren Division (NSWCDD). This report has been reviewed at NSWCDD by R. Neal Cain, Head, Combat Systems Technology Group and by Frank Rucky, Head, Digital Systems Branch.

Approved by:

MARY E. LACEY, Head
Systems Research and Technology Department

CONTENTS

ILLUSTRATIONS

ILLUSTRATIONS (continued)

1.0 INTRODUCTION

Alignment is the process of calibrating a sensor relative to some standard. Specifically, it determines the bias or offset errors in the sensor by comparing the data reported by the sensor to the standard. Alignment is usually classified as either **absolute** or **relative**, depending on the type of standard. This classification is somewhat artificial since any alignment procedure is fundamentally a relative process; that is, alignment relative to some standard. However, a useful distinction can be made between absolute and relative alignment. The standard used in absolute alignment contains no bias errors with respect to some universal standard. Thus, the sensor-reported data can be correctly expressed relative to the universal standard by absolutely aligning the sensor. However, in relative alignment, the standard may contain some bias errors with respect to the universal standard. In this case, the sensor-reported data cannot be correctly expressed relative to the universal standard. Whether this is a problem will depend on the application. For example, if the various sensors in a multisensor system are relatively aligned to the same standard, then all of the multisensor data can be correctly expressed relative to the common standard, even though this common standard may contain bias errors with respect to the universal standard. This may be sufficient for the operation of the multisensor system.

This report will focus on the absolute alignment of the positional data reported by a tracking sensor. Typically, alignment must be considered in tracking applications whenever it is desired to express the track data reported by the sensor in another reference frame. For example, alignment

considerations occur in multisensor tracking applications when it is desired to express the multisensor track data in a common reference frame, which is required in constructing a unified track picture of the environment. The track data reported by an aligned sensor can be correctly transformed to any reference frame that is also aligned to the standard. For an unaligned sensor, the presence of any uncompensated alignment errors will produce errors in the sensor's data when it is transformed to another frame. These uncompensated alignment errors may seriously degrade the performance of a sensor system. For example, alignment errors in a multisensor tracking system can cause a single target to be reported at different locations by the various sensors so that it appears to be multiple targets. The degradation of performance in a multisensor tracking system due to uncompensated alignment errors is documented in Conte and Helmick[1] using simple simulations.

One source of alignment errors is bias errors in the measurements reported by the tracking sensor. Although the sensor is usually calibrated in an initial calibration procedure, the calibration may deteriorate over time. Another source of alignment errors is attitude (or orientation) bias errors. Most sensors incorporate some technique to stabilize their data by determining the attitude of the sensor (e.g., with a gyroscopic device). Attitude bias errors can be caused by offset and drift errors in the gyros. Other sources of alignment errors include sensor location bias errors caused by offset and drift errors in the navigation systems associated with the sensors and timing bias errors in the clocks for the sensors. Figure 1-1 illustrates the effects of range bias and bearing bias errors in a radar on a target position reported by the radar. In this case, an alignment procedure would attempt to estimate the range and bearing bias errors by comparing the positional data reported by the radar to some standard. Once these bias errors are estimated, they can be removed from the positional data reported by the radar.

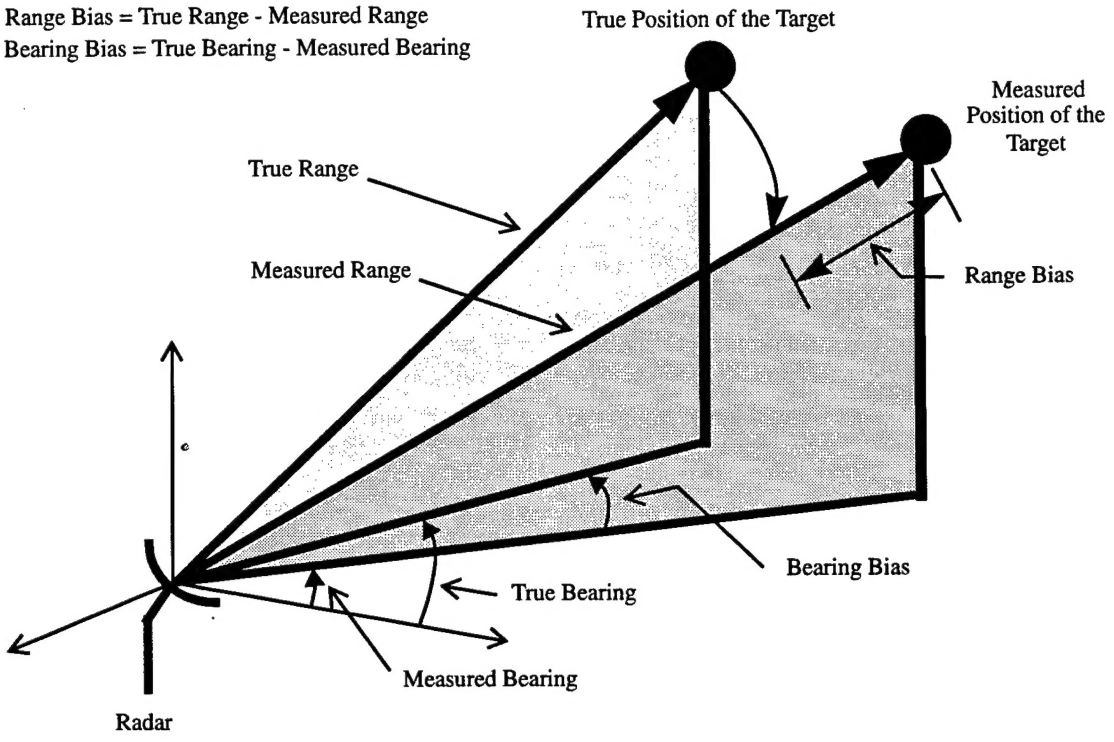

FIGURE 1-1. EFFECTS OF RANGE AND BEARING BIASES ON THE POSITION OF A TARGET

For relative alignment in multisensor tracking systems, one of the sensors is usually chosen as the standard and the other sensors are aligned to it. The sensor chosen as the standard is called the *master* or *primary* sensor and it is assumed to be free of bias errors. The master sensor is made *observable* to the other sensors via overlapping coverage zones that contain tracks of common targets. The targets that are mutually held by a sensor and the master sensor are used to determine the biases that will relatively align the sensor to the master sensor. This also explains the popularity of relative alignment procedures; that is, the ready availability of mutual track data bases. A potential problem with relative alignment is that the master sensor may not actually be free of bias errors and thus relative alignment will produce a true alignment that is no better than the alignment accuracy of the master sensor. Whether this is a problem will depend on the application.

Another problem with relative alignment can arise if data from remote sources are brought into the local integrated multisensor system, where the remote sensor reporting the data is not observable to the master sensor. Conversely, problems can also arise if data from the local integrated system are sent to remote systems.

In tracking applications, relative alignment procedures have been very popular because of the previous lack of absolute or universal standards and the ready availability of relative standards such as mutual track data bases. However, with the advent of GPS (Global Positioning System), standards that closely approximate truth are currently available. GPS receivers are inexpensive and accurate, and the constellation of GPS satellites will soon be observable worldwide. Thus, it should be possible to use GPS as an absolute standard for sensor alignment.

One possible technique using GPS for absolute alignment can be described as follows. A cooperative target would be equipped with a GPS receiver to precisely determine its location. A communications link to transmit its GPS-derived location to the sensor that is being absolutely aligned would be required. It would be necessary for the sensor to track the cooperative target and report its position. Also, the sensor to be aligned would be equipped with a GPS receiver to precisely determine its location.† The absolute alignment technique would compare the cooperative target's position as reported by the sensor to its GPS-derived position. Any differences between the sensor-reported and GPS-derived positions would be attributed to bias errors in the track data reported by the sensor. Here, the GPS-derived position serves as the absolute standard to which the sensor-reported positions are aligned.

† The track data reported by the sensor is typically expressed in a reference frame whose origin is attached to the sensor. However, the GPS-derived target position is usually expressed in an earth-centered frame. Comparison of the GPS-derived target position to the sensor-reported target position will require the transformation of the GPS-derived position to the reference frame located at the sensor or *vice versa*. This transformation requires the precise location of the sensor, which could also be determined using GPS.

This technique has the potential for achieving an accurate absolute alignment. It should be fairly simple to implement from an algorithmic point of view. In multisensor applications, the technique would avoid the problem of needing overlapping coverage zones if all of the sensors employed this technique; the integration of sensor data from remote sources into the local multi-sensor system and *vice versa* would be less of a problem; and the technique would be applicable to widely distributed sensors as well as co-located sensors.

The purpose of this report is to develop an algorithm for absolutely aligning the positional data reported by a tracking sensor using a target whose location is measured by the sensor and whose location can also be precisely determined independently of the sensor's measurements. This algorithm also requires the location of the sensor to be accurately known. As stated above, GPS is one candidate for providing precise location information for both the target and the sensor. However, the algorithm is applicable to any technique that provides precise location information independently of the sensor's measurements.

This absolute alignment algorithm will consist of two basic functions or modules: (1) the bias estimation module, and (2) the bias correction module. The purpose of the bias estimation module is to estimate the bias errors using the difference between the target's sensor-reported position and the target's precise position that is determined independently of the sensor's measurements. The bias correction module will receive estimates of the bias errors from the bias estimation module and then use these bias estimates to compensate (or correct) for the effects of the bias errors in the sensor's data. That is, the bias correction module will absolutely align all of the tracks reported by the sensor, not only the track of the target used to estimate the biases.

The main steps in constructing these two modules are to model the bias errors and then develop equations that relate the modeled bias errors to the true and sensor-reported positions of a

target. The bias estimation module will apply known filtering techniques to estimate the biases. Specifically, the bias estimation module will employ two Kalman filters: a filter to estimate the range bias and another one to estimate the angular biases. The bias correction module will then absolutely align any target track reported by the sensor using the estimated biases from the bias estimation module.

The absolute alignment algorithm will require data from several sources: the system providing the precise location of a target independently of the sensor's measurements; the system providing the precise location of the sensor; the position of the target that is reported by the sensor; and possibly the attitude of the sensor if it is determined using a sensing device (e.g., a gyroscopic device). This multisource data will most likely be asynchronous. Since the alignment algorithm will require time-coincident or synchronized data, estimation algorithms (i.e., filtering and prediction) will be required to extrapolate at least some of the various multisource data to a common point in time. The estimation algorithm used to filter the multisource data and predict the multisource filtered states to a common point in time is not the focus of this report, and it will not be examined further. It will be assumed that synchronized estimates of the multisource data are available for processing in the alignment algorithm.

This report is organized as follows. Section 2 presents background material on stabilizing the data reported by a sensor. Section 3 presents the modeling of the bias errors and the development of the absolute alignment algorithm. Simulation results are presented in Section 4 to illustrate the performance of the alignment algorithm. Section 5 summarizes the results of this effort.

2.0 STABILIZATION

2.1 INTRODUCTION

The measurements reported by a sensor will be meaningful and useful only if they are expressed relative to a known reference. That is, a reference frame is necessary for describing the measurements reported by a sensor. A reference frame is usually characterized by three axes and the location of its origin, which is the point of intersection of the three axes. One of the reference frames associated with a sensor is its *measurement frame*. The measurement frame is the frame in which the sensor's measurements are actually obtained. The origin of the measurement frame is located at the sensor and its axes are often defined by the architecture of the sensor or of the platform on which the sensor resides. For example, in shipboard applications, the axes of the measurement frame are often formed by the fore-aft line, the horizontal line that is orthogonal to the fore-aft line, and the axis that is orthogonal to the horizontal plane formed by the other two. The measurement frame rotates about all three of its axes as the sensor rotates in pitch, roll, and yaw, and thus it is considered non-inertial and it is said to be *unstabilized*. One source of the rotations of the measurement frame in pitch, roll, and yaw can be the flexure and/or motion of the platform on which the sensor resides.

Although a sensor's measurements are actually obtained in its unstabilized measurement frame, it is often better to transform the measurements to an inertial or nonrotating frame, or to a frame that is a fairly good approximation to an inertial frame. The *stabilized frame* is the reference

frame for a sensor that serves as an inertial frame or an approximation to an inertial frame. *Stabilization* refers to the process of compensating for the attitude (or orientation) of a sensor's measurement frame with respect to its stabilized frame. In targeting and tracking applications, the stabilized frame is often the local tangent frame whose origin is located at the sensor's position on the earth and whose axes are formed by the true north-south horizontal line, the true east-west horizontal line, and the axis that is orthogonal to the horizontal plane formed by the north-south and east-west lines. Since this frame rotates with the earth, it is only an approximation to an inertial reference frame.

The stabilized frame at a particular point on the earth is illustrated in Figure 2-1. The axes of the stabilized frame are represented by three mutually orthogonal vectors, where one of the vectors points eastward, one points northward, and the final one points in the direction of an outward normal vector (i.e., in the "up" direction). As Figure 2-1 suggests, the orientation of the stabilized frame depends on its location on the earth; that is, the orientation changes at different points on the earth.

Stabilization is usually achieved by a device (such as a gimbal) that mechanically maintains the alignment of the sensor to its stabilized frame, or by measuring the attitude of the sensor and then using this attitude to transform the sensor's data to its stabilized frame using mathematical computations. Specifically, the stabilization technique can be grouped into three major classes:[2]

- *Unstabilized* - The sensor operates in a totally unstable environment and its data contain rotational components (e.g., pitch, roll, and yaw) with respect to its stabilized frame. Any compensation is external to the sensor using a device to sense the attitude of the sensor with respect to its stabilized frame. This attitude is then used to transform the sensor's data to its stabilized frame using mathematical computations.

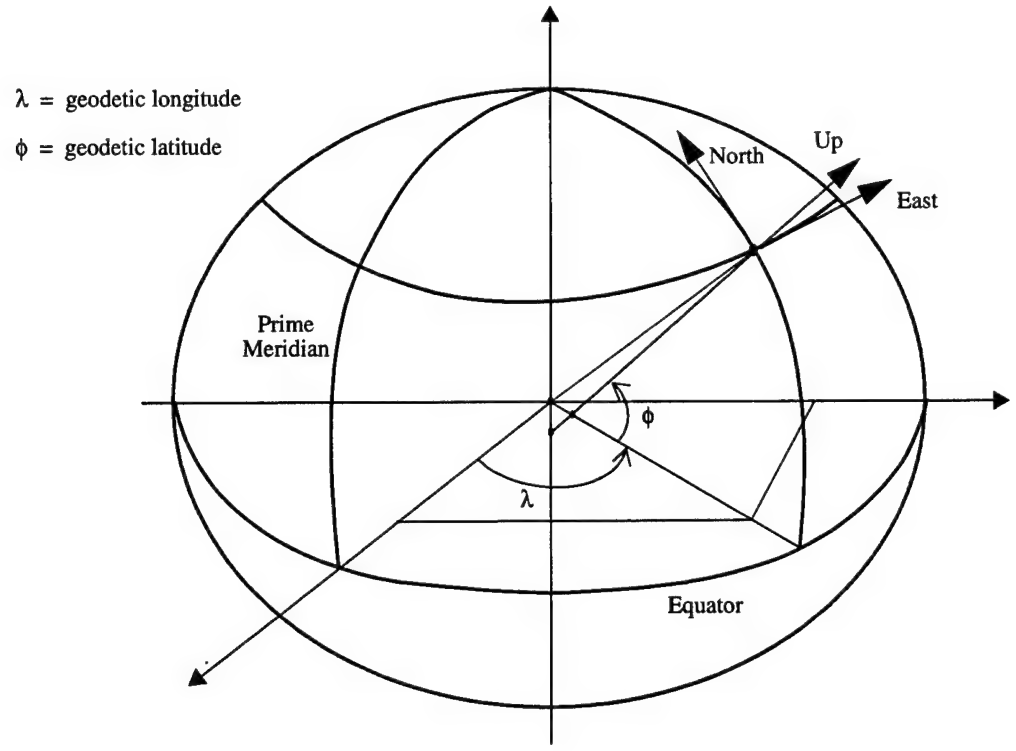

FIGURE 2-1. STABILIZED FRAME (EAST, NORTH, UP) AT A PARTICULAR POINT ON THE EARTH

- *Partially Stabilized* - The sensor is mechanically stabilized along one axis using some device, and its data contain rotational components in the remaining (unstabilized) axes. Any compensation along the unstabilized axes is external to the sensor and accomplished in a manner similar to the unstabilized case.

- *Fully Stabilized* - The sensor is gimbal-mounted and the alignment of the sensor to its stabilized frame is mechanically maintained. Thus, the sensor's data contain no rotational components with respect to its stabilized frame and no further compensation is required.

Most tracking sensors that provide positional measurements for targets can be classified into four distinct types depending on the type of positional measurements they provide:

(1) range, bearing, and elevation;

(2) range and bearing;

(3) bearing and elevation;

(4) bearing.

For example, a precision tracking radar usually provides measurements of range, bearing, and elevation, while a surveillance radar may only provide range and bearing. A passive infrared search and tracking sensor usually provides bearing and elevation, and an acoustical sensor may only provide bearing measurements.

If the sensor is not fully mechanically stabilized, then any stabilization of the unstabilized axes will be external to the sensor using transformation equations and the measured attitude of the sensor. The transformation equations for the stabilization are examined below. It is possible to stabilize sensor classes 1 and 3, while classes 2 and 4 can not be truly stabilized using only equations because they do not provide enough information to determine the three-dimensional position of a target nor the unit direction vector to a target. Although class 3 does not provide full three-dimensional positional information, it does provide enough information to determine the unit direction vector to a target and this unit direction vector can be stabilized.

2.2 TRANSFORMATION EQUATIONS

To uniquely describe a position in a specific reference frame requires the introduction of a system of coordinates. Since the sensor is assumed to provide measurements of range, bearing,

and elevation, it is natural to use a spherical coordinate system to describe a position. The spherical coordinate system used in this report is illustrated in Figure 2-2 and it employs a linear distance and two angles to describe a position. The range R is the distance along the straight line from the sensor (which is located at the origin O) to the target, the bearing B is the angle measured from the Y axis in the horizontal plane formed by the X and Y axes, and the elevation E is the angle measured above the horizontal plane. For example, in the stabilized frame illustrated in Figure 2-1, the X axis points eastward, the Y axis points northward, and the Z axis points in the "up" direction. Thus, the bearing is measured from the north direction in the stabilized frame of Figure 2-1. It will be useful to introduce a rectangular (or cartesian) coordinate system in a reference frame. The rectangular coordinate system is also illustrated in Figure 2-2. It employs three linear distances to describe the position of a target; that is, the distances X, Y, and Z along the X, Y, and Z axes, respectively.

Coordinate conversion is the process of changing from one set of coordinates that describes a point in a reference frame to another system of coordinates describing the same point in the same reference frame.[2] Thus, if the spherical coordinates R, B, and E are specified in a reference frame, the conversion to the rectangular coordinates X, Y, and Z in the same reference frame is computed using the following three equations:

$$X = R \cos E \sin B \tag{2-1}$$

$$Y = R \cos E \cos B \tag{2-2}$$

$$Z = R \sin E \tag{2-3}$$

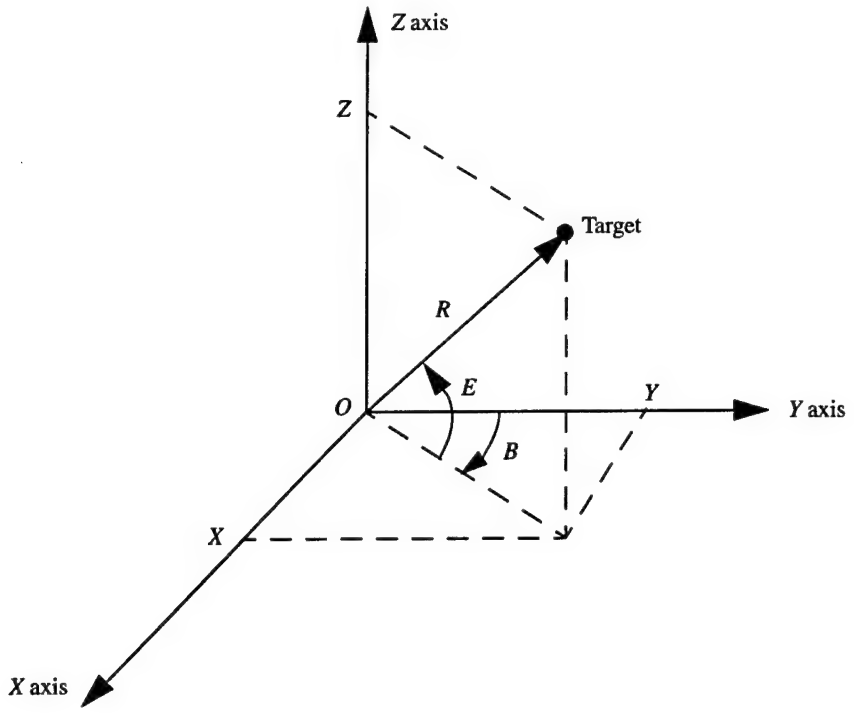

FIGURE 2-2. SPHERICAL AND RECTANGULAR COORDINATES IN THE SAME REFERENCE FRAME

Conversely, if the rectangular coordinates X, Y, and Z are specified, the conversion to the spherical coordinates R, B, and E is computed using the following three equations:

$$R = \sqrt{X^2 + Y^2 + Z^2} \tag{2-4}$$

$$B = \tan^{-1}\left(\frac{X}{Y}\right) \tag{2-5}$$

$$E = \sin^{-1}\left(\frac{Z}{R}\right) \tag{2-6}$$

The process of stabilization of a target's position is one of transforming the target's coordinates from the unstabilized measurement frame to the stabilized frame using the same coordinate system.[2] Both frames have the same origin, but one is tilted with respect to the other one. This transformation is most easily described using rectangular coordinates. The transformation between these frames can be described by a set of Eulerian angles. The *xyz-convention*[3] is used in this report. In the xyz-convention, the transformation from the stabilized frame to the unstabilized measurement frame is accomplished by first rotating about the Z axis of the stabilized frame by the yaw angle y, then rotating about the intermediate Y axis by the pitch angle p, and rotating about the final X axis by the roll angle r (see Figure 2-3). The transformation from the unstabilized measurement frame to the stabilized frame is obtained by reversing the above rotations.

Let X_S, Y_S, and Z_S denote the rectangular coordinates of a point in the stabilized frame. Rotating about the Z axis of the stabilized frame by the yaw angle y produces the coordinates X_I, Y_I, and Z_I in an intermediate reference frame, which are computed by

$$X_I = X_S \cos y + Y_S \sin y \tag{2-7}$$

$$Y_I = -X_S \sin y + Y_S \cos y \tag{2-8}$$

$$Z_I = Z_S \tag{2-9}$$

Rotating about the Y_I axis by the pitch angle p produces the set of coordinates X_{II}, Y_{II}, and Z_{II}, which are computed by

$$X_{II} = X_I \cos p - Z_I \sin p \tag{2-10}$$

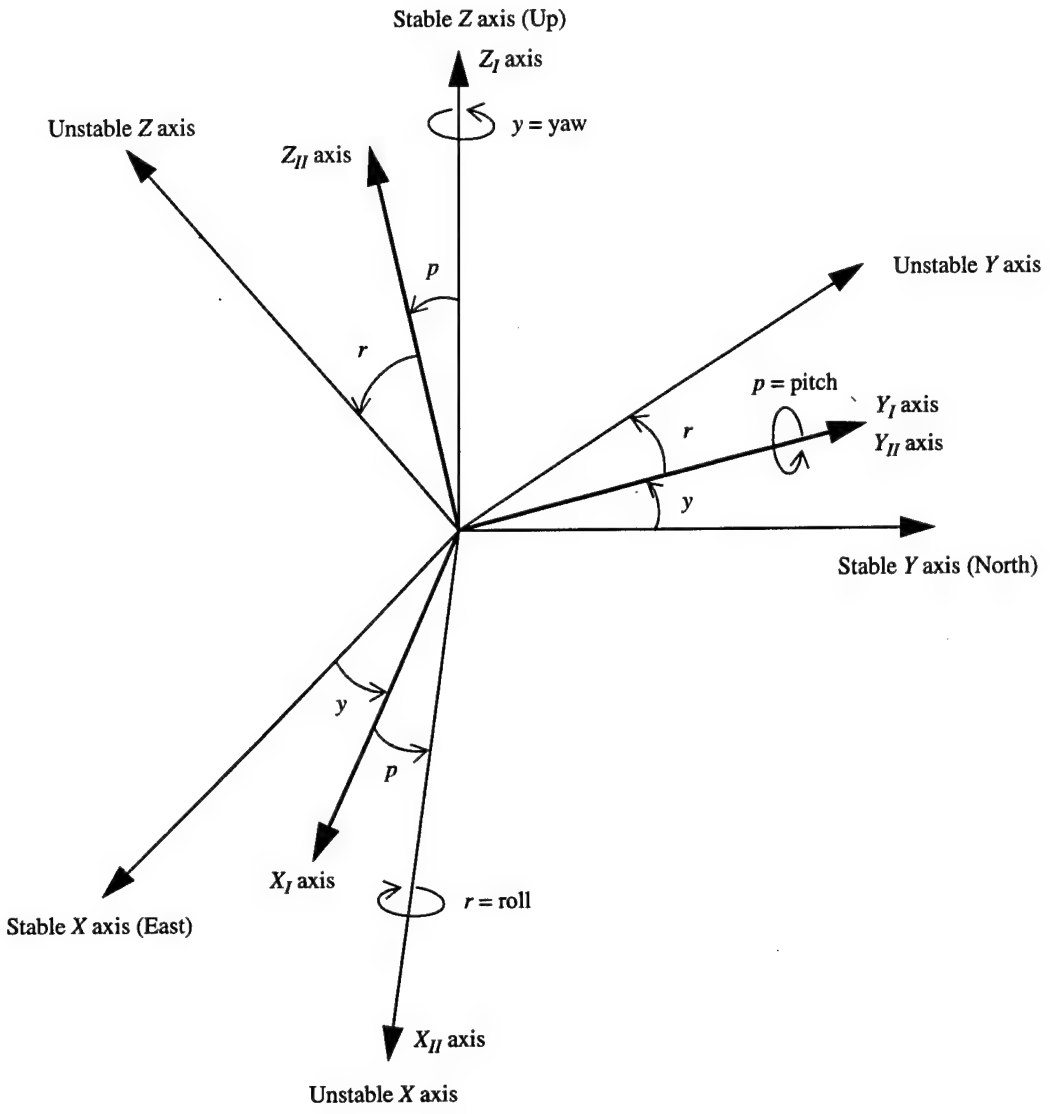

FIGURE 2-3. UNSTABILIZED MEASUREMENT AND STABILIZED FRAMES ALONG WITH THE YAW, PITCH, AND ROLL ANGLES

$$Y_{II} = Y_I \tag{2-11}$$

$$Z_{II} = X_I \sin p + Z_I \cos p \tag{2-12}$$

Finally, rotating about the X_{II} axis by the roll angle r produces the set of (unstabilized) coordinates X_U, Y_U, and Z_U in the measurement frame, which are computed by

$$X_U = X_{II} \tag{2-13}$$

$$Y_U = Y_{II}\cos r + Z_{II}\sin r \tag{2-14}$$

$$Z_U = -Y_{II}\sin r + Z_{II}\cos r \tag{2-15}$$

The three rotational transformations above can be expressed in matrix notation by the following three equations:

$$\begin{bmatrix} X_I \\ Y_I \\ Z_I \end{bmatrix} = \begin{bmatrix} \cos y & \sin y & 0 \\ -\sin y & \cos y & 0 \\ 0 & 0 & 1 \end{bmatrix} \begin{bmatrix} X_S \\ Y_S \\ Z_S \end{bmatrix} = \boldsymbol{B}_{yaw} \begin{bmatrix} X_S \\ Y_S \\ Z_S \end{bmatrix} \tag{2-16}$$

$$\begin{bmatrix} X_{II} \\ Y_{II} \\ Z_{II} \end{bmatrix} = \begin{bmatrix} \cos p & 0 & -\sin p \\ 0 & 1 & 0 \\ \sin p & 0 & \cos p \end{bmatrix} \begin{bmatrix} X_I \\ Y_I \\ Z_I \end{bmatrix} = \boldsymbol{B}_{pitch} \begin{bmatrix} X_I \\ Y_I \\ Z_I \end{bmatrix} \tag{2-17}$$

$$\begin{bmatrix} X_U \\ Y_U \\ Z_U \end{bmatrix} = \begin{bmatrix} 1 & 0 & 0 \\ 0 & \cos r & \sin r \\ 0 & -\sin r & \cos r \end{bmatrix} \begin{bmatrix} X_{II} \\ Y_{II} \\ Z_{II} \end{bmatrix} = \boldsymbol{B}_{roll} \begin{bmatrix} X_{II} \\ Y_{II} \\ Z_{II} \end{bmatrix} \tag{2-18}$$

where $\boldsymbol{B}_{yaw}$, $\boldsymbol{B}_{pitch}$, and $\boldsymbol{B}_{roll}$ are each 3 x 3 orthogonal matrices. Combining these three equations into a single vector equation gives the transformation from the stabilized frame to the unstabilized measurement frame as

$$\boldsymbol{r}_U = \boldsymbol{B}\boldsymbol{r}_S \tag{2-19}$$

where

$$\boldsymbol{r}_U = \begin{bmatrix} X_U \\ Y_U \\ Z_U \end{bmatrix} \qquad \boldsymbol{r}_S = \begin{bmatrix} X_S \\ Y_S \\ Z_S \end{bmatrix} \tag{2-20}$$

and

$$\begin{aligned} \boldsymbol{B} = \boldsymbol{B}_{roll}\boldsymbol{B}_{pitch}\boldsymbol{B}_{yaw} &= \begin{bmatrix} 1 & 0 & 0 \\ 0 & \cos r & \sin r \\ 0 & -\sin r & \cos r \end{bmatrix}\begin{bmatrix} \cos p & 0 & -\sin p \\ 0 & 1 & 0 \\ \sin p & 0 & \cos p \end{bmatrix}\begin{bmatrix} \cos y & \sin y & 0 \\ -\sin y & \cos y & 0 \\ 0 & 0 & 1 \end{bmatrix} \\ &= \begin{bmatrix} \cos p\cos y & \cos p\sin y & -\sin p \\ (\sin p\sin r\cos y - \cos r\sin y) & (\sin p\sin r\sin y + \cos r\cos y) & \cos p\sin r \\ (\sin p\cos r\cos y + \sin r\sin y) & (\sin p\cos r\sin y - \sin r\cos y) & \cos p\cos r \end{bmatrix} \end{aligned} \tag{2-21}$$

The transformation from the unstabilized measurement frame to the stabilized frame is obtained by reversing the above rotations:

$$\boldsymbol{r}_S = \boldsymbol{A}\boldsymbol{r}_U \tag{2-22}$$

where

$$\begin{aligned} \boldsymbol{A} = \boldsymbol{A}_{yaw}\boldsymbol{A}_{pitch}\boldsymbol{A}_{roll} &= \begin{bmatrix} \cos y & -\sin y & 0 \\ \sin y & \cos y & 0 \\ 0 & 0 & 1 \end{bmatrix}\begin{bmatrix} \cos p & 0 & \sin p \\ 0 & 1 & 0 \\ -\sin p & 0 & \cos p \end{bmatrix}\begin{bmatrix} 1 & 0 & 0 \\ 0 & \cos r & -\sin r \\ 0 & \sin r & \cos r \end{bmatrix} \\ &= \begin{bmatrix} \cos p\cos y & (\sin p\sin r\cos y - \cos r\sin y) & (\sin p\cos r\cos y + \sin r\sin y) \\ \cos p\sin y & (\sin p\sin r\sin y + \cos r\cos y) & (\sin p\cos r\sin y - \sin r\cos y) \\ -\sin p & \cos p\sin r & \cos p\cos r \end{bmatrix} \end{aligned} \tag{2-23}$$

and

$$\boldsymbol{A}_{yaw} = \boldsymbol{B}_{yaw}^{T} \qquad \boldsymbol{A}_{pitch} = \boldsymbol{B}_{pitch}^{T} \qquad \boldsymbol{A}_{roll} = \boldsymbol{B}_{roll}^{T} \qquad \boldsymbol{A} = \boldsymbol{B}^{T} \tag{2-24}$$

where the superscript T denotes matrix transpose. Equation (2-22) is the transformation that stabilizes a target's position using rectangular coordinates.

It is also possible to develop a transformation that stabilizes a target's position using spherical coordinates. Let R_S, B_S, and E_S denote the spherical coordinates of a point in the stabilized frame, and let R_U, B_U, and E_U denote the (unstabilized) spherical coordinates of a point in the measurement frame. Here, R_U, B_U, and E_U are the target's range, bearing, and elevation that are reported by the sensor in its (unstabilized) measurement frame.

Using the equations above, it can be shown that the range is invariant with respect to the stabilizing transformation; that is,

$$R_S = \sqrt{X_S^2 + Y_S^2 + Z_S^2} = \sqrt{X_U^2 + Y_U^2 + Z_U^2} = R_U \tag{2-25}$$

The stabilized bearing B_S is defined by

$$B_S = \tan^{-1}\left(\frac{X_S}{Y_S}\right) \tag{2-26}$$

It can be shown that

$$B_S = \tan^{-1}\left(\frac{X_I \cos y - Y_I \sin y}{X_I \sin y + Y_I \cos y}\right) = \tan^{-1}\left(\frac{(X_I/Y_I) - \tan y}{1 + (X_I/Y_I)\tan y}\right) \tag{2-27}$$

Defining the bearing B_I (in the intermediate frame formed by the X_I, Y_I, and Z_I axes) by

$$\tan B_I = X_I / Y_I \tag{2-28}$$

allows Equation (2-27) to be expressed as

$$B_S = \tan^{-1}\left(\frac{\tan B_I - \tan y}{1 + \tan B_I \tan y}\right) = \tan^{-1}\left[\tan\left(B_I - y\right)\right] = B_I - y \tag{2-29}$$

The bearing B_I in Equation (2-28) is also given by

$$\begin{aligned} B_I &= \tan^{-1}\left(\frac{X_I}{Y_I}\right) = \tan^{-1}\left(\frac{X_{II}\cos p + Z_{II}\sin p}{Y_{II}}\right) \\ &= \tan^{-1}\left(\frac{X_U\cos p + \left(Y_U\sin r + Z_U\cos r\right)\sin p}{Y_U\cos r - Z_U\sin r}\right) \\ &= \tan^{-1}\left(\frac{\cos E_U\sin B_U\cos p + \left(\cos E_U\cos B_U\sin r + \sin E_U\cos r\right)\sin p}{\cos E_U\cos B_U\cos r - \sin E_U\sin r}\right) \end{aligned} \tag{2-30}$$

The stabilized elevation E_S is defined by

$$E_S = \sin^{-1}\left(\frac{Z_S}{R_S}\right) \tag{2-31}$$

It can be shown that

$$\begin{aligned} E_S &= \sin^{-1}\left(\frac{Z_I}{R_U}\right) = \sin^{-1}\left(\frac{-X_{II}\sin p + Z_{II}\cos p}{R_U}\right) \\ &= \sin^{-1}\left(\frac{-X_U\sin p + \left(Y_U\sin r + Z_U\cos r\right)\cos p}{R_U}\right) \\ &= \sin^{-1}\left\{-\cos E_U\sin B_U\sin p + \left(\cos E_U\cos B_U\sin r + \sin E_U\cos r\right)\cos p\right\} \end{aligned} \tag{2-32}$$

In summary, the transformation that stabilizes the target's position using spherical coordinates is given by the following equations:

$$R_S = R_U \tag{2-33}$$

$$B_S = B_I - y \tag{2-34}$$

$$E_S = \sin^{-1}\{-\cos E_U \sin B_U \sin p + (\cos E_U \cos B_U \sin r + \sin E_U \cos r)\cos p\} \tag{2-35}$$

where

$$B_I = \tan^{-1}\left(\frac{\cos E_U \sin B_U \cos p + (\cos E_U \cos B_U \sin r + \sin E_U \cos r)\sin p}{\cos E_U \cos B_U \cos r - \sin E_U \sin r}\right) \tag{2-36}$$

Note that the stabilization of the bearing and elevation does not require the range; it only requires the unstabilized bearing and unstabilized elevation along with the yaw, pitch, and roll angles.

The transformation from the stabilized frame to the unstabilized measurement frame using spherical coordinates can also be obtained in a similar manner, and it is given by the following equations:

$$R_U = R_S \tag{2-37}$$

$$B_U = \tan^{-1}\left(\frac{\sin(B_S + y)\cos p - \tan E_S \sin p}{\cos(B_S + y)\cos r + [\sin(B_S + y)\sin p + \tan E_S \cos p]\sin r}\right) \tag{2-38}$$

$$E_U = \sin^{-1}\{\cos E_S \cos(B_S + y)\sin r + [\cos E_s \sin(B_S + y)\sin p + \sin E_S \cos p]\cos r\} \tag{2-39}$$

Equation (2-22) is the transformation that stabilizes a target's position using rectangular coordinates and Equations (2-33) to (2-36) are the corresponding transformation equations using spherical coordinates. These equations require the range, bearing, and elevation (or their rectangular counterparts) reported by the sensor, along with the yaw, pitch, and roll angles, which are measured using some device that senses the attitude of the sensor. Thus, these equations are applicable to a sensor reporting range, bearing, and elevation. Also, since Equations (2-34) to (2-36) do not require the range, they can be used to stabilize a sensor only reporting bearing and elevation. However, it is not possible to truly stabilize a sensor only reporting range and bearing using transformation equations because the stabilization of the bearing in Equations (2-34) and (2-36) requires the elevation. This also applies to a sensor only reporting bearing.

For a sensor only reporting range and bearing, or a sensor only reporting bearing, the best solution is to have a gimbal-mounted sensor (i.e., a fully mechanically stabilized sensor) so that the sensor's data contain no rotational components with respect to the stabilized frame and thus no further compensation (i.e., no transformation equation) is required. If this is not possible, then all that can be done is to assign an arbitrary value to the elevation and use the above transformation equations to "pseudo-stabilize" the sensor. For example, one could let the elevation be zero in the above equations. Of course, for targets with moderate to large elevations, this pseudo-stabilization procedure may produce a "stabilized" bearing that is more unstable than the unstabilized bearing reported by the sensor.

3.0 ABSOLUTE ALIGNMENT ALGORITHM

3.1 INTRODUCTION

The absolute alignment algorithm is developed in this section. This algorithm will consist of two basic modules: (1) the bias estimation module, and (2) the bias correction module. The purpose of the bias estimation module is to estimate the bias errors using the difference between a target's sensor-reported position and its precise position as determined by some absolute standard that is independent of the sensor's measurements. The bias correction module will receive estimates of the bias errors from the bias estimation module and then use these bias estimates to correct for the effects of the bias errors in the sensor's data. The structure of the alignment algorithm will depend on the locations of the bias correction and bias estimation modules relative to the sensor's tracking module. Various architectures are possible and they will be discussed in Section 3.2. This is followed in Section 3.3 by a brief overview of the modeling of the bias errors. Section 3.4 presents the development of the equations that relate the modeled bias errors to the true and sensor-reported positions of a target. A linearized version of the alignment model is presented in Section 3.5 and the nonlinear model is presented in Section 3.6. This is followed in Section 3.7 by a discussion of the bias estimation module. The estimation of the bias errors will use two filters: one to estimate the range bias and another one to estimate the angular biases. Finally, Section 3.8 presents the equations needed in the bias correction module to absolutely align the various classes of sensors.

3.2 ALIGNMENT ARCHITECTURES

Various architectures for integrated alignment and tracking systems are possible depending on the locations of the bias correction and bias estimation modules relative to the sensor's tracking module. For example, block diagrams for two possible architectures implementing GPS-based absolute alignment techniques are illustrated in Figures 3-1 and 3-2. Each of the figures depicts a cooperative target equipped with a GPS receiver (RCVR) and a transmitter (XMTR) which broadcasts its GPS-derived state to the sensor. The sensor is also equipped with a GPS receiver to determine its state. An attitude sensing device (e.g., a gyroscopic device) is used to determine the attitude state of the sensor (if the sensor is not equipped with an attitude sensing device, then it is assumed that the sensor is gimbal-mounted and thus fully mechanically stabilized). The sensor's measurements are stabilized in the stabilization module using the attitude state.

A *track-alignment* architecture is illustrated in Figure 3-1. Both the bias estimation and the bias correction are performed after the sensor-reported measurements have been processed in the sensor's tracking module. That is, the measurements reported by the sensor are not aligned before they are processed in the sensor's tracking module. The estimation and correction of the biases are performed at the track level rather than at the measurement level. Such an architecture would be needed for those situations where it was not possible to alter the data processing functions internal to the sensor's system. Rather, one would only have access to the sensor's track data base, which would be unaligned. However, one would still need estimates of the sensor's attitude state to implement the track-alignment architecture. The cooperative target's unaligned track, along with the estimates of the attitude state and the GPS-derived states of the sensor and cooperative target, are used in the bias estimation module to estimate the biases. The estimated biases are then used

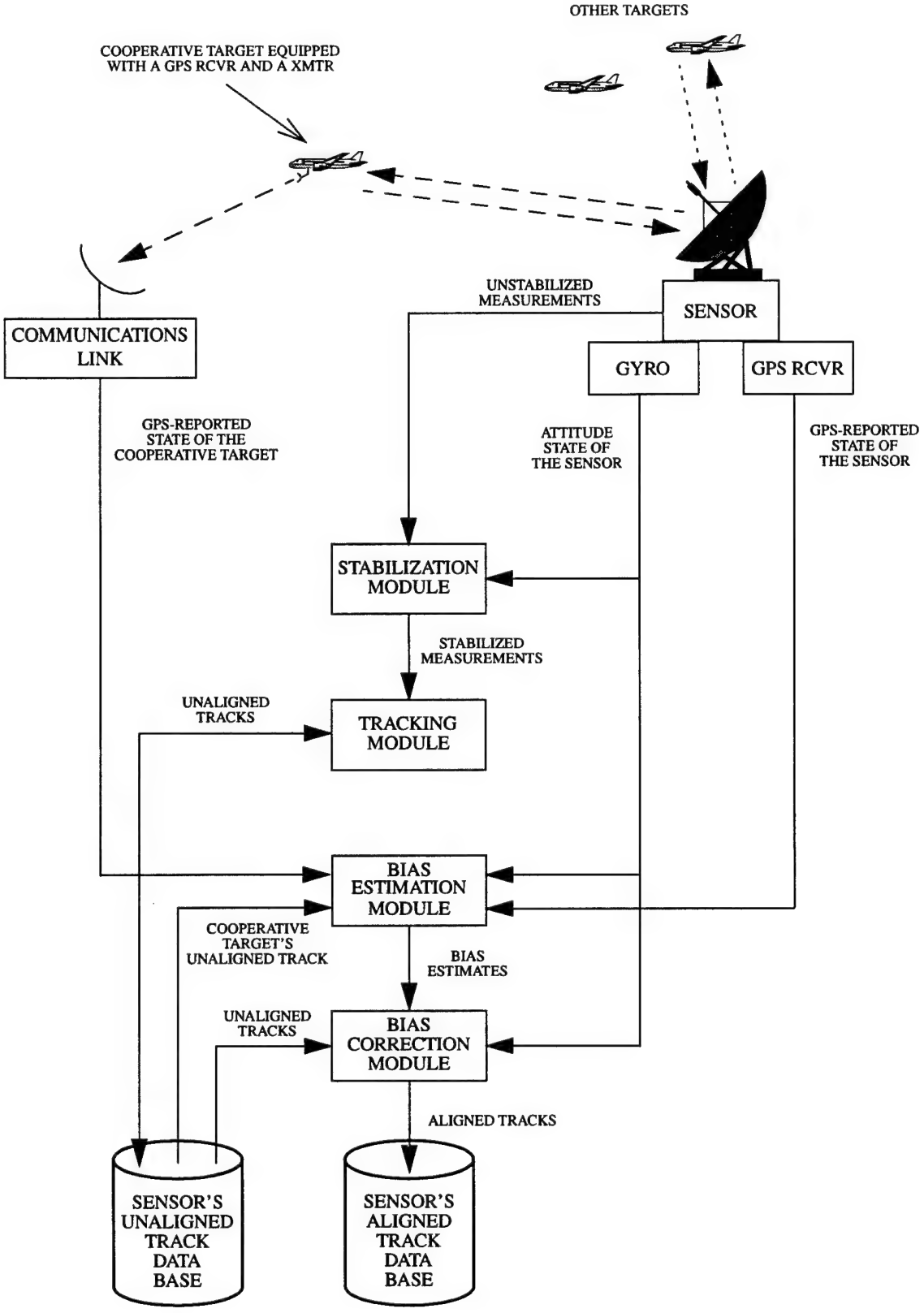

FIGURE 3-1. TRACK-ALIGNMENT ARCHITECTURE

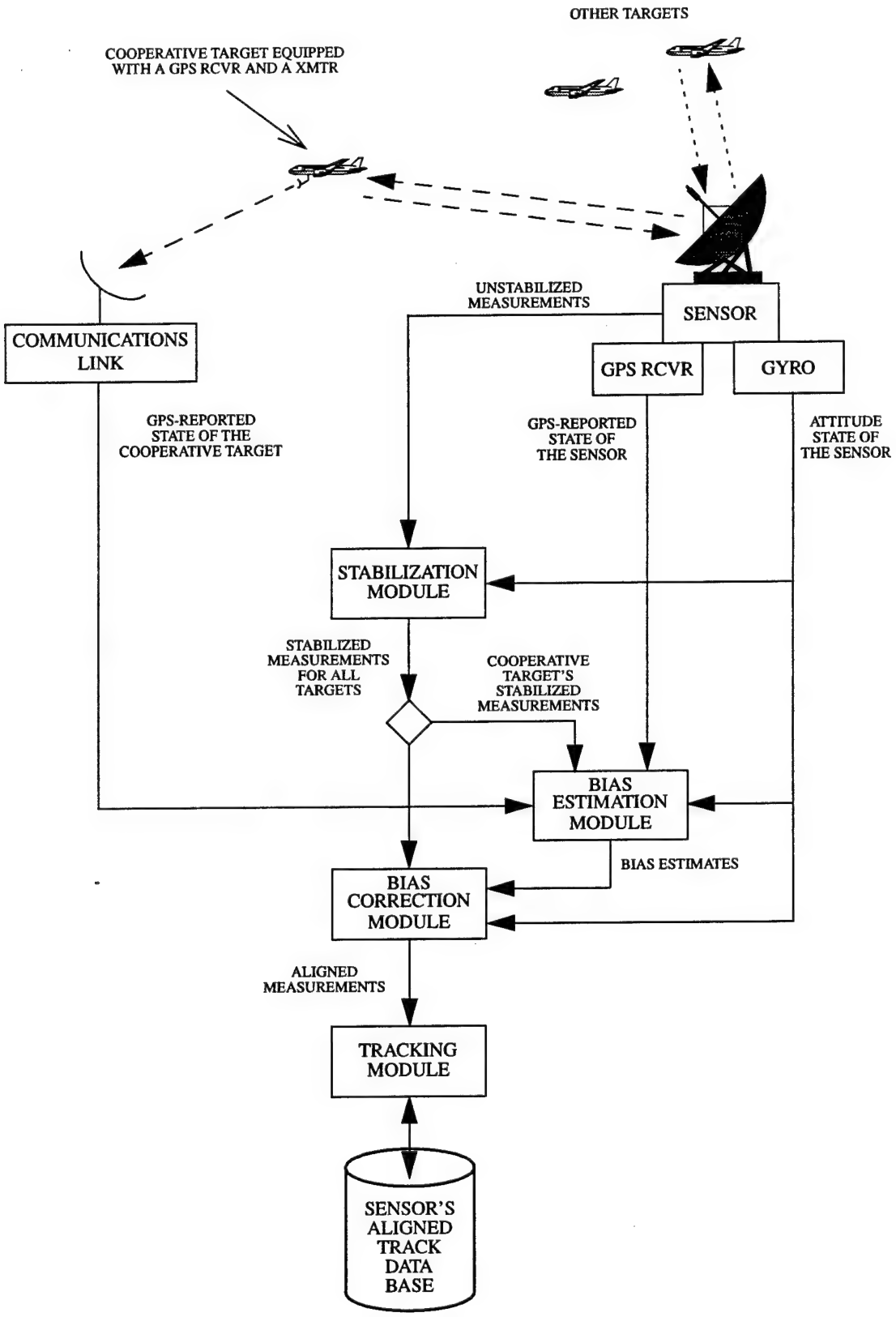

FIGURE 3-2. MEASUREMENT-ALIGNMENT ARCHITECTURE

in the bias correction module to align all of the tracks in the sensor's track data base. Note that this technique will result in two track data bases: the unaligned track data base, and the aligned track data base. The two track data bases are required because the sensor's tracking module processes measurements that have not been aligned. Serious degradation in tracking performance can occur if an attempt is made to use aligned tracks and unaligned measurements in the tracking module.

If it is possible to alter the data processing functions internal to the sensor's system, then one could align the measurements reported by the sensor before they are processed in the sensor's tracking module. Such a *measurement-alignment* architecture is illustrated in Figure 3-2. Here, the estimation and correction of the biases are performed immediately after the stabilization of the measurements. Only one track data base would be required because the sensor's tracking module processes measurements that have been aligned, and thus this track data base would also be aligned. Another possible measurement alignment architecture would perform the estimation and correction of the biases before the stabilization of the measurements.

3.3 MODELING OF THE BIAS ERRORS

The bias errors will be modeled as additive offsets to the reported values of the quantities. Temporarily ignoring the random errors in the system, the equations modeling the bias errors are given by

$$R_U^{true}(t) = R_U(t) + R_{bias}(t) \tag{3-1}$$

$$B_U^{true}(t) = B_U(t) + B_{bias}(t) \tag{3-2}$$

$$E_U^{true}(t) = E_U(t) + E_{bias}(t) \tag{3-3}$$

$$p^{true}(t) = p(t) + p_{bias}(t) \tag{3-4}$$

$$r^{true}(t) = r(t) + r_{bias}(t) \tag{3-5}$$

$$y^{true}(t) = y(t) + y_{bias}(t) \tag{3-6}$$

In these equations, $R_U(t)$, $B_U(t)$, and $E_U(t)$ are the target's (unstabilized) spherical coordinates that are reported by the sensor at time t; $p(t)$, $r(t)$, and $y(t)$ are the attitude angles that give the sensor's orientation at time t; $R_U^{true}(t)$, $B_U^{true}(t)$, $E_U^{true}(t)$, $p^{true}(t)$, $r^{true}(t)$, and $y^{true}(t)$ are the corresponding true values at time t; and $R_{bias}(t)$, $B_{bias}(t)$, $E_{bias}(t)$, $p_{bias}(t)$, $r_{bias}(t)$, and $y_{bias}(t)$ are the bias errors at time t.

Equations (3-1) to (3-3) for the range, bearing, and elevation are expressed in the unstabilized measurement frame because the biases in these quantities are assumed to be caused by offsets in the (spherical) measurements reported by the sensor. Since these measurements occur in the unstabilized measurement frame of the sensor, it is appropriate to model the bias errors in the unstabilized measurement frame. Depending on the type of architecture employed, the target's sensor-reported spherical coordinates $R_U(t)$, $B_U(t)$, and $E_U(t)$ in Equations (3-1) to (3-3) can be either measured values or filtered values. In the measurement-alignment architecture, they refer to the (unstabilized) measured values, but in the track-alignment architecture they refer to the tracked or filtered values (but expressed in the unstabilized measurement frame).

3.4 RELATIONSHIP BETWEEN THE MODELED BIAS ERRORS AND THE TRUE AND SENSOR-REPORTED POSITIONS OF A TARGET

The relationship between the modeled bias errors and the true and reported positions of a target can be developed either in rectangular coordinates or in spherical coordinates. Simulations have shown that a scaling problem may arise if all of the biases are estimated in a single filter based on a linear approximation developed in rectangular coordinates. The reason is that a linear distance (i.e., the range bias) and angular quantities (i.e., the angular biases) are estimated in a single filter. If the alignment error due to the range bias is much smaller than the alignment error caused by the angular biases, then it is extremely difficult to obtain precise range bias estimates. However, it is possible to manipulate the equations so that the range bias decouples from the angular biases. This decoupling has the salutary effect of negating any scaling problems that may occur because the decoupling allows the range bias to be estimated independently of the angular biases and *vice versa*. For the relative alignment problem considered by Helmick *et al.*,[4-7] this decoupling is accomplished by first linearizing the equations in rectangular coordinates by assuming that the bias errors are small quantities and using a first-order Taylor series expansion. Manipulations of the linearized equations are then performed to express them in spherical coordinates, which results in the range bias equation decoupling from the angular bias equations and *vice versa*. Since this is a circuitous route to obtaining the alignment equations in spherical coordinates, it is easier to develop the alignment relationships in spherical coordinates from the beginning using the transformations shown in Equations (2-33) to (2-36). Here, the range bias and angular biases will be decoupled from the beginning. Also, no smallness assumptions on the range bias and angular biases are required. This is the approach that will be followed below.

The transformation that stabilizes the target's reported position in spherical coordinates using the reported attitude angles is given by Equations (2-33) to (2-36). These equations can be expressed as

$$R_S = R_U \tag{3-7}$$

$$B_S = f(B_U, E_U, p, r, y) \tag{3-8}$$

$$E_S = g(B_U, E_U, p, r) \tag{3-9}$$

where the functions f and g are defined by

$$f(B_U, E_U, p, r, y) = \tan^{-1}\left\{\frac{u(B_U, E_U, p, r)}{v(B_U, E_U, r)}\right\} - y \tag{3-10}$$

$$g(B_U, E_U, p, r) = \sin^{-1}\{w(B_U, E_U, p, r)\} \tag{3-11}$$

and the functions u, v, and w are defined by

$$u(B_U, E_U, p, r) = \cos E_U \sin B_U \cos p + (\cos E_U \cos B_U \sin r + \sin E_U \cos r)\sin p \tag{3-12}$$

$$v(B_U, E_U, r) = \cos E_U \cos B_U \cos r - \sin E_U \sin r \tag{3-13}$$

$$w(B_U, E_U, p, r) = -\cos E_U \sin B_U \sin p + (\cos E_U \cos B_U \sin r + \sin E_U \cos r)\cos p \tag{3-14}$$

For simplicity, we have dropped the time notation t introduced in Section 3.3. All of the quantities in the above equations are assumed to be valid at time t.

The transformation that stabilizes the target's true position in spherical coordinates using the true attitude angles is given by the following equations

$$R_S^{true} = R_U^{true} \tag{3-15}$$

$$B_S^{true} = f\ (B_U^{true}, E_U^{true}, p^{true}, r^{true}, y^{true}) \tag{3-16}$$

$$E_S^{true} = g\,(B_U^{true}, E_U^{true}, p^{true}, r^{true}) \tag{3-17}$$

Substituting Equations (3-1) to (3-7) into these equations gives

$$R_S^{true} = R_S + R_{bias} \tag{3-18}$$

$$B_S^{true} = f(B_U + B_{bias}, E_U + E_{bias}, p + p_{bias}, r + r_{bias}, y + y_{bias}) \tag{3-19}$$

$$E_S^{true} = g\,(B_U + B_{bias}, E_U + E_{bias}, p + p_{bias}, r + r_{bias}) \tag{3-20}$$

Equations (3-18) to (3-20) are the fundamental equations for absolute alignment. They relate the modeled bias errors to the true and reported positions of a target in spherical coordinates. Note that Equation (3-18) for the range bias is decoupled from Equations (3-19) and (3-20) for the angular biases, and *vice versa*. Also, the range bias equation is a linear function of the range bias, while the remaining two equations are nonlinear functions of the angular biases.

If the estimates of the biases are available, these three equations can be used to align the positions of the targets reported by the sensor. In this case, the true values of the range, bearing,

and elevation will represent the aligned positional coordinates in the stabilized frame. Conversely, if the above equations are used to estimate the biases, the true values of the range, bearing, and elevation that are required for a target in the stabilized frame are assumed to be available from an absolute standard such as GPS. However, simulations have shown that observability problems are encountered if an attempt is made to estimate all of the angular biases. In particular, it is difficult to separate the effects of the bearing and yaw biases in the data. The basic problem is that the orientations of the stabilized frame and the unstabilized measurement frame are only slightly different when the magnitudes of the pitch and roll angles are small and, in this case, the bearing and yaw biases represent rotations about axes that are nearly parallel. This difficulty is most easily demonstrated by examining the linearized versions of the above alignment equations.

3.5 LINEAR ALIGNMENT MODEL

A linearized version of the alignment equations will be obtained by assuming that the magnitudes of the angular biases are small quantities and by using a first-order Taylor series expansion in Equations (3-19) and (3-20). Note that Equation (3-18) for the range bias is already linear and thus it does not have to be linearized. The linear alignment model will be applicable to those situations where the magnitudes of the angular bias errors are small.

Expanding Equations (3-19) and (3-20) about the reported values of the quantities using a first-order Taylor series expansion gives the following approximations to the angular alignment equations:

$$
\begin{aligned}
B_S^{true} &\approx f(B_U, E_U, p, r, y) + (\partial f/\partial B_U) \cdot B_{bias} + (\partial f/\partial E_U) \cdot E_{bias} + \\
&\quad (\partial f/\partial p) \cdot p_{bias} + (\partial f/\partial r) \cdot r_{bias} + (\partial f/\partial y) \cdot y_{bias} \\
&= B_S + (\partial f/\partial B_U) \cdot B_{bias} + (\partial f/\partial E_U) \cdot E_{bias} + \\
&\quad (\partial f/\partial p) \cdot p_{bias} + (\partial f/\partial r) \cdot r_{bias} + (\partial f/\partial y) \cdot y_{bias}
\end{aligned} \tag{3-21}
$$

$$
\begin{aligned}
E_S^{true} &\approx g(B_U, E_U, p, r) + (\partial g/\partial B_U) \cdot B_{bias} + (\partial g/\partial E_U) \cdot E_{bias} + \\
&\quad (\partial g/\partial p) \cdot p_{bias} + (\partial g/\partial r) \cdot r_{bias} \\
&= E_S + (\partial g/\partial B_U) \cdot B_{bias} + (\partial g/\partial E_U) \cdot E_{bias} + \\
&\quad (\partial g/\partial p) \cdot p_{bias} + (\partial g/\partial r) \cdot r_{bias}
\end{aligned} \tag{3-22}
$$

where all of the partial derivatives are evaluated at the reported values of the quantities (i.e., at R_U, B_U, E_U, p, r, and y). These partial derivatives are obtained by differentiating Equations (3-10) to (3-14) with respect to the appropriate variable, and they are given by

$$\frac{\partial f}{\partial B_U} = \left(\frac{1}{u^2 + v^2}\right)\left[v\,\frac{\partial u}{\partial B_U} - u\,\frac{\partial v}{\partial B_U}\right] \qquad \frac{\partial g}{\partial B_U} = \frac{1}{\sqrt{1 - w^2}} \cdot \frac{\partial w}{\partial B_U} \tag{3-23}$$

$$\frac{\partial f}{\partial E_U} = \left(\frac{1}{u^2 + v^2}\right)\left[v\,\frac{\partial u}{\partial E_U} - u\,\frac{\partial v}{\partial E_U}\right] \qquad \frac{\partial g}{\partial E_U} = \frac{1}{\sqrt{1 - w^2}} \cdot \frac{\partial w}{\partial E_U} \tag{3-24}$$

$$\frac{\partial f}{\partial p} = \left(\frac{1}{u^2 + v^2}\right)\left[v\,\frac{\partial u}{\partial p} - u\,\frac{\partial v}{\partial p}\right] \qquad \frac{\partial g}{\partial p} = \frac{1}{\sqrt{1 - w^2}} \cdot \frac{\partial w}{\partial p} \tag{3-25}$$

$$\frac{\partial f}{\partial r} = \left(\frac{1}{u^2 + v^2}\right)\left[v\,\frac{\partial u}{\partial r} - u\,\frac{\partial v}{\partial r}\right] \qquad \frac{\partial g}{\partial r} = \frac{1}{\sqrt{1 - w^2}} \cdot \frac{\partial w}{\partial r} \tag{3-26}$$

$$\frac{\partial f}{\partial y} = -1 \qquad \frac{\partial g}{\partial y} = 0 \tag{3-27}$$

and

$$\frac{\partial u}{\partial B_U} = \alpha \cdot \cos E_U \qquad \frac{\partial v}{\partial B_U} = -\cos E_U \sin B_U \cos r \qquad \frac{\partial w}{\partial B_U} = -\beta \cdot \cos E_U \tag{3-28}$$

$$\frac{\partial u}{\partial E_U} = -\sin E_U \sin B_U \cos p - \gamma \cdot \sin p \qquad \frac{\partial v}{\partial E_U} = -\zeta$$
$$\frac{\partial w}{\partial E_U} = \sin E_U \sin B_U \sin p - \gamma \cdot \cos p \tag{3-29}$$

$$\frac{\partial u}{\partial p} = w \qquad \frac{\partial v}{\partial p} = 0 \qquad \frac{\partial w}{\partial p} = -u \tag{3-30}$$

$$\frac{\partial u}{\partial r} = v \cdot \sin p \qquad \frac{\partial v}{\partial r} = -\eta \qquad \frac{\partial w}{\partial r} = v \cdot \cos p \tag{3-31}$$

and

$$\alpha = \cos B_U \cos p - \sin B_U \sin r \sin p \qquad \beta = \cos B_U \sin p + \sin B_U \sin r \cos p \tag{3-32}$$

$$\gamma = \sin E_U \cos B_U \sin r - \cos E_U \cos r \qquad \zeta = \sin E_U \cos B_U \cos r + \cos E_U \sin r \tag{3-33}$$

$$\eta = \cos E_U \cos B_U \sin r + \sin E_U \cos r \tag{3-34}$$

Simulations have shown that observability problems are encountered if an attempt is made to estimate all of the angular biases. The problem is that it is difficult to estimate both the bearing and yaw biases. This is due to the orientations of the stabilized frame and the unstabilized measurement frame being only slightly different when the magnitudes of the pitch and roll angles are small. In this case, the bearing and yaw biases represent rotations about axes that are nearly parallel.

This observability problem is most easily demonstrated by examining the coefficients for the biases in Equations (3-21) and (3-22). Assuming that the magnitudes of the pitch and roll angles are small, the first-order approximations of the bias terms in Equations (3-21) and (3-22) are given by

$$\begin{aligned} (\partial f/\partial B_U) \cdot B_{bias} &\approx B_{bias} & (\partial f/\partial E_U) \cdot E_{bias} &\approx 0 \\ (\partial f/\partial p) \cdot p_{bias} &\approx (\tan E_U \cos B_U)\, p_{bias} & (\partial f/\partial y) \cdot y_{bias} &= -y_{bias} \\ (\partial f/\partial r) \cdot r_{bias} &\approx (\tan E_U \sin B_U)\, r_{bias} \end{aligned} \tag{3-35}$$

$$\begin{aligned} (\partial g/\partial B_U) \cdot B_{bias} &\approx 0 & (\partial g/\partial E_U) \cdot E_{bias} &\approx E_{bias} \\ (\partial g/\partial p) \cdot p_{bias} &\approx -(\sin B_U)\, p_{bias} & (\partial g/\partial r) \cdot r_{bias} &\approx (\cos B_U)\, r_{bias} \end{aligned} \tag{3-36}$$

In this case, the linear angular alignment equations reduce to

$$B_S^{true} \approx B_S + (B_{bias} - y_{bias}) + (\tan E_U \cos B_U)\, p_{bias} + (\tan E_U \sin B_U)\, r_{bias} \tag{3-37}$$

$$E_S^{true} \approx E_S + E_{bias} - (\sin B_U)\, p_{bias} + (\cos B_U)\, r_{bias} \tag{3-38}$$

It is clear from these equations that the bearing bias and the yaw bias are linearly dependent when the magnitudes of the pitch and roll angles are small. Rather than futilely attempting to estimate the individual bearing and yaw biases, this implies that it is more appropriate to estimate an azimuth bias A_{bias}, which is the linear combination given by

$$A_{bias} = B_{bias} - y_{bias}, \tag{3-39}$$

when the pitch and roll angles are small. In simulations, problems have been encountered in estimating the bearing and yaw biases even for pitch and roll angles of large magnitudes. Thus, Equation (3-39) will be used even if the magnitudes of the pitch and roll angles are not small.

The azimuth bias A_{bias} includes the effects of both the bearing bias B_{bias} and the yaw bias y_{bias}. The question remains as to how the azimuth bias will be used in the alignment equations. It will be modeled as an additive offset to the bearing; that is, Equation (3-2) becomes

$$B_U^{true} = B_U + A_{bias} \tag{3-40}$$

Since the azimuth bias includes the effects of the yaw bias, the true yaw angle in Equation (3-6) becomes

$$y^{true} = y \tag{3-41}$$

Thus, the general linear alignment model is given by the following three equations:

$$R_S^{true} = R_S + R_{bias} \tag{3-42}$$

$$\begin{aligned} B_S^{true} = B_S + (\partial f/\partial B_U) \cdot A_{bias} + (\partial f/\partial E_U) \cdot E_{bias} + \\ (\partial f/\partial p) \cdot p_{bias} + (\partial f/\partial r) \cdot r_{bias} \end{aligned} \tag{3-43}$$

$$\begin{aligned} E_S^{true} = E_S + (\partial g/\partial B_U) \cdot A_{bias} + (\partial g/\partial E_U) \cdot E_{bias} + \\ (\partial g/\partial p) \cdot p_{bias} + (\partial g/\partial r) \cdot r_{bias} \end{aligned} \tag{3-44}$$

This linear alignment model will be applicable to those situations where the magnitudes of the angular bias errors are small. Note that it does not require any smallness assumption on the magnitude of the range bias.

3.6 NONLINEAR ALIGNMENT MODEL

The general nonlinear alignment model from Section 3.4 is now given by the following three equations:

$$R_S^{true} = R_S + R_{bias} \tag{3-45}$$

$$B_S^{true} = f(B_U + A_{bias}, E_U + E_{bias}, p + p_{bias}, r + r_{bias}, y) \tag{3-46}$$

$$E_S^{true} = g(B_U + A_{bias}, E_U + E_{bias}, p + p_{bias}, r + r_{bias}) \tag{3-47}$$

These equations relate the modeled bias errors to the true position and the sensor-reported position of a target using spherical coordinates. Note that no smallness assumptions on the range bias and angular biases are required in the above nonlinear alignment model.

3.7 BIAS ESTIMATION MODULE

The bias estimation module produces estimates of the bias errors by comparing a target's sensor-reported position to its precise position as determined by some absolute standard. The fundamental equations used to develop the filters in the bias estimation module are Equations (3-45) to (3-47) for the nonlinear alignment model or Equations (3-42) to (3-44) for the linear model. In the bias estimation module, these equations are applied to one or more sensor-reported targets whose positions can also be determined by some absolute standard that is independent of the sensor's measurements.

The true position of the target is modeled as the sum of its position as determined by some absolute standard plus a random error term. That is, the true (rectangular coordinate) position vector $\boldsymbol{r}_S^{true}$ in the (true) stabilized frame of the sensor is given by†

$$\boldsymbol{r}_S^{true} = \boldsymbol{r}_S^{std} + \boldsymbol{e}_{r_S}^{std} \tag{3-48}$$

where $\boldsymbol{r}_S^{std}$ is the (rectangular coordinate) position vector of the target that is determined using the absolute standard and $\boldsymbol{e}_{r_S}^{std}$ is the corresponding random error in the absolute standard. Assuming that the magnitude of the random error vector is small, the first-order approximation of Equation (3-48) in spherical coordinates can be expressed as

$$R_S^{true} = R_S^{std} + e_{R_S}^{std} \tag{3-49}$$

$$B_S^{true} = B_S^{std} + e_{B_S}^{std} \tag{3-50}$$

$$E_S^{true} = E_S^{std} + e_{E_S}^{std} \tag{3-51}$$

where R_S^{std}, B_S^{std}, and E_S^{std} are the range, bearing, and elevation of the target based on the abso-

† Since the alignment will be performed in the stabilized frame whose origin is attached to the sensor, the position vectors and error vector in Equation (3-48) are assumed to be expressed in this stabilized frame. However, the target position as determined by the absolute standard will probably be expressed in another frame (e.g., an earth-centered frame if GPS is used as the absolute standard). Thus, it is assumed that the transformation of the target position as determined by the absolute standard to the stabilized frame has been previously performed and it is available for use in Equation (3-48). Note that this transformation needs the location of the sensor, which leads to our requirement that the precise location of the sensor is also determined using an absolute standard.

lute standard, and $e_{R_S}^{std}$, $e_{B_S}^{std}$, and $e_{E_S}^{std}$ are the corresponding random errors. The statistics of these random errors are assumed known.

Using Equations (3-49) to (3-51) in Equations (3-45) to (3-47), the nonlinear alignment model can now be expressed as

$$R_S^{std} = R_S + R_{bias} + (e_{R_U} - e_{R_S}^{std}) \tag{3-52}$$

$$\begin{aligned} B_S^{std} = f(&B_U + A_{bias} + e_{B_U}, E_U + E_{bias} + e_{E_U}, p + p_{bias} + e_p, \\ &r + r_{bias} + e_r, y + e_y) - e_{B_S}^{std} \end{aligned} \tag{3-53}$$

$$\begin{aligned} E_S^{std} = g(&B_U + A_{bias} + e_{B_U}, E_U + E_{bias} + e_{E_U}, \\ &p + p_{bias} + e_p, r + r_{bias} + e_r) - e_{E_S}^{std} \end{aligned} \tag{3-54}$$

where we have included the random errors e_{R_U}, e_{B_U}, e_{E_U}, e_p, e_r, and e_y in the sensor-reported positions and the attitude angles. The statistics of these random errors are assumed known.

Assuming that the magnitudes of these random errors are small, the first-order approximation of the nonlinear model is given by

$$R_S^{std} - R_S = R_{bias} + e_R \tag{3-55}$$

$$B_S^{std} = f(B_U + A_{bias}, E_U + E_{bias}, p + p_{bias}, r + r_{bias}, y) + e_B \tag{3-56}$$

$$E_S^{std} = g(B_U + A_{bias}, E_U + E_{bias}, p + p_{bias}, r + r_{bias}) + e_E \tag{3-57}$$

where the random error terms e_R, e_B, and e_E can be shown to be given by

$$e_R = e_{R_S} - e_{R_S}^{std} \tag{3-58}$$

$$e_B = e_{B_S} - e_{B_S}^{std} \tag{3-59}$$

$$e_E = e_{E_S} - e_{E_S}^{std} \tag{3-60}$$

and e_{R_S}, e_{B_S}, and e_{E_S} are the errors in the sensor-reported data in the stabilized frame, which are given by

$$e_{R_S} = e_{R_U} \tag{3-61}$$

$$\begin{aligned} e_{B_S} = {} & (\partial f/\partial B_U) \cdot e_{B_U} + (\partial f/\partial E_U) \cdot e_{E_U} + (\partial f/\partial p) \cdot e_p + \\ & (\partial f/\partial r) \cdot e_r + (\partial f/\partial y) \cdot e_y \end{aligned} \tag{3-62}$$

$$e_{E_S} = (\partial g/\partial B_U) \cdot e_{B_U} + (\partial g/\partial E_U) \cdot e_{E_U} + (\partial g/\partial p) \cdot e_p + (\partial g/\partial r) \cdot e_r \tag{3-63}$$

Ignoring any correlations between the random errors in the ranges and the random errors in the angular quantities allows us to use two decoupled filters to estimate the biases. A linear Kalman filter[8,9] can be used to estimate the range bias, where Equation (3-55) serves as the linear measurement equation. (This also assumes a linear dynamical model for the range bias.) An extended Kalman filter[8,9] or an iterated extended Kalman filter[8,9] can be used to estimate the angular biases, where Equations (3-56) and (3-57) serve as the nonlinear measurement equations.

Alternatively, using Equation (3-49) to (3-51) in Equations (3-42) to (3-44) gives the linear alignment model as

$$R_S^{std} - R_S = R_{bias} + e_R \tag{3-64}$$

$$\begin{aligned} B_S^{std} - B_S = {} & (\partial f/\partial B_U) \cdot A_{bias} + (\partial f/\partial E_U) \cdot E_{bias} + \\ & (\partial f/\partial p) \cdot p_{bias} + (\partial f/\partial r) \cdot r_{bias} + e_B \end{aligned} \tag{3-65}$$

$$\begin{aligned} E_S^{std} - E_S = {} & (\partial g/\partial B_U) \cdot A_{bias} + (\partial g/\partial E_U) \cdot E_{bias} + \\ & (\partial g/\partial p) \cdot p_{bias} + (\partial g/\partial r) \cdot r_{bias} + e_E \end{aligned} \tag{3-66}$$

Again, ignoring any correlations between the random errors in the ranges and the random errors in the angular quantities allows us to use two decoupled filters to estimate the biases. A linear Kalman filter can be used to estimate the range bias, where Equation (3-64) serves as the linear measurement equation. A linear Kalman filter can also be used to estimate the angular biases, where Equations (3-65) and (3-66) serve as the linear measurement equations. (This also assumes a linear dynamical model for the angular biases.)

One or more targets are designated for use in the bias estimation module to determine the values of the bias errors. The positions of these targets must be reported by the sensor and, in addition, the positions of these targets must also be provided by some absolute standard that is independent of the sensor's measurements. One cycle of the bias estimation processing for one of these targets is briefly summarized in the following steps:

1. The estimation of the biases using the target's sensor-reported position at time t begins with the following spherical coordinates in the stabilized frame:

$$R_S(t), B_S(t), E_S(t)$$

In the measurement-alignment architecture, these are the (stabilized) positional measurements, but in the track-alignment architecture they represent the track-level positional data. The covariances for the errors in these quantities are assumed known. For the track-alignment architecture, these covariances are usually supplied by the tracking filter. However, for the measurement-alignment architecture, they can be computed using Equations (3-61) to (3-63) and the assumed covariances for the (unstabilized) sensor-reported measurements and the covariances in the attitude states.

2. Obtain the attitude state, the state of the target as determined by the absolute standard, and the state of the sensor as determined by the absolute standard that are valid at time t. This may require either extrapolation or interpolation of the available states to time t. In any case, the following are assumed available at time t:

Attitude Angles: $p(t), r(t), y(t)$

Target's Position Vector from the Absolute Standard: $\mathbf{r}^{std}_{target}(t)$

Sensor's Position Vector from the Absolute Standard: $\mathbf{r}^{std}_{sensor}(t)$

The covariances for the uncertainties in these quantities are assumed known.

3. The position vectors $\boldsymbol{r}_{target}^{std}(t)$ and $\boldsymbol{r}_{sensor}^{std}(t)$ are used to compute the position vector $\boldsymbol{r}_S^{std}(t)$ of the target in the stabilized frame of the sensor.‡ The position vector $\boldsymbol{r}_S^{std}(t)$ is then converted to spherical coordinates, which gives $R_S^{std}(t)$, $B_S^{std}(t)$, and $E_S^{std}(t)$. The covariances for the errors in these quantities are assumed known.

4. Use Equations (2-37) to (2-39) to transform $R_S(t), B_S(t), E_S(t)$ (from Step 1) to the unstabilized measurement frame, which gives

$$R_U(t), B_U(t), E_U(t)$$

5. The bias estimates and corresponding covariances from the previous bias estimation cycle are predicted to time t using the assumed dynamical model for the biases.

6. The predicted bias estimates, the attitude state, the absolutely-determined (spherical) coordinates of the target, and the sensor-reported (spherical) coordinates of the target are used to update the biases at time t. A linear Kalman filter is used to estimate the range bias, where

‡ For example, if the position vectors $\boldsymbol{r}_{target}^{std}$ and $\boldsymbol{r}_{sensor}^{std}$, which are determined using some absolute standard, are rectangular position vectors that are expressed in an earth-centered frame, then

$$\boldsymbol{r}^{std} = \boldsymbol{r}_{target}^{std} - \boldsymbol{r}_{sensor}^{std}$$

is the position vector of the target relative to the sensor. The vector $\boldsymbol{r}^{std}$ is in the reference frame that is parallel to the earth-centered frame and whose origin is located at the sensor. This vector can be rotated into the stabilized frame of the sensor using the transformation

$$\boldsymbol{r}_S^{std} = \boldsymbol{A}\boldsymbol{r}^{std}$$

where $\boldsymbol{r}_S^{std}$ is the position vector of the target in the sensor's stabilized frame and $\boldsymbol{A}$ is the rotation matrix given by

$$\boldsymbol{A} = \begin{bmatrix} -\sin\lambda & \cos\lambda & 0 \\ -\cos\lambda\sin\phi & -\sin\lambda\sin\phi & \cos\phi \\ \cos\lambda\cos\phi & \sin\lambda\cos\phi & \sin\phi \end{bmatrix}$$

where λ and ϕ are the longitude and latitude for the sensor, respectively.

Equation (3-55) is used as the measurement equation. If an extended Kalman filter or an iterated extended Kalman filter is used to estimate the angular biases, then Equations (3-56) and (3-57) are used as the measurement equations. If a linear Kalman is used to estimate the angular biases, then Equations (3-65) and (3-66) are used as the measurement equations. Equations (3-58) to (3-60) can be used to compute the covariances for the measurement noise terms in these equations.

The above bias estimation procedure applies to a sensor measuring range, bearing, and elevation. For a sensor only measuring bearing and elevation, the same angular bias filter as described in Step 6 above is used; however, no range bias filter is required. For a sensor only measuring range and bearing, Step 6 uses the same linear Kalman filter to estimate the range bias, but uses only Equation (3-56) to estimate the angular biases for the nonlinear model or Equation (3-65) for the linear model. The elevation $E_S(t)$ is needed in Step 4 for the computation of $B_U(t)$ and $E_U(t)$. Since $E_S(t)$ is not provided by a sensor only measuring range and bearing, one lets $E_S(t) = E_S^{std}(t)$ in Step 4 for this case. That is, the elevation as determined by the absolute standard is assigned to the target's sensor-reported position. This also implies that the elevation bias is zero and thus it does not have to be estimated. Finally, for a sensor only measuring the bearing, no range bias filter is required, and Equation (3-56) is used in the angular bias filter for the nonlinear model or Equation (3-65) for the linear model. Again, since $E_S(t)$ is not provided, one lets $E_S(t) = E_S^{std}(t)$ in Step 4 and no elevation bias is estimated.

3.8 BIAS CORRECTION MODULE

Once bias estimates are available from the bias estimation module, the bias correction module is used to absolutely align all of the sensor's data using the estimated biases. Note that the bias correction module aligns the data for all of the targets reported by the sensor, not only the target(s) used to estimate the biases. The alignment of any sensor-reported target data in the bias correction module is summarized in the following steps:

1. The absolute alignment of any target's data at time t starts with its sensor-reported (spherical) position in the stabilized frame:

$$R_S(t), B_S(t), E_S(t)$$

   In the measurement-alignment architecture, these are the (stabilized) positional measurements, but in the track-alignment architecture they represent the track-level positional data.

2. Obtain the attitude state of the sensor and the bias estimates that are valid at time t. This may require either extrapolation or interpolation of the available attitude states and bias estimates to time t. In any case, the following are assumed to be available at time t:

   Attitude Angles: $p(t), r(t), y(t)$

   Bias Estimates: $\hat{R}_{bias}(t), \hat{A}_{bias}(t), \hat{E}_{bias}(t), \hat{p}_{bias}(t), \hat{r}_{bias}(t)$

3. Use Equations (2-37) to (2-39) to transform $R_S(t), B_S(t), E_S(t)$ (from Step 1) to the unstabilized measurement frame at time t, which gives

$$R_U(t), B_U(t), E_U(t)$$

4. Absolutely align the (spherical) positional data using the following equations:

$$R_S^{aligned}(t) = R_U(t) + \hat{R}_{bias}(t) \tag{3-67}$$

$$B_S^{aligned}(t) = f\ (B_U(t) + \hat{A}_{bias}(t), E_U(t) + \hat{E}_{bias}(t), p(t) + \hat{p}_{bias}(t), r(t) + \hat{r}_{bias}(t), y(t)\ ) \tag{3-68}$$

$$E_S^{aligned}(t) = g\,(B_U(t) + \hat{A}_{bias}(t), E_U(t) + \hat{E}_{bias}(t), p(t) + \hat{p}_{bias}(t), r(t) + \hat{r}_{bias}(t)\ ) \tag{3-69}$$

where $R_S^{aligned}(t)$, $B_S^{aligned}(t)$, and $E_S^{aligned}(t)$ represent the absolutely aligned positional data in the stabilized frame.

The above bias correction procedure applies to a sensor reporting range, bearing, and elevation. The above procedure also applies to a sensor only reporting bearing and elevation if Equation (3-67) is ignored. However, for a sensor only reporting range and bearing, or a sensor only reporting bearing, then all that can be done is to "pseudo-align" the bearing. For example, one could assign arbitrary values (e.g., zeros) to the required elevation and elevation bias in the bearing alignment equation.

4.0 SIMULATIONS

4.1 INTRODUCTION

The absolute alignment algorithm was tested by simulating a tracking sensor and including both bias and random errors in the data reported by the sensor. The algorithm was tested for a tracking sensor measuring range, bearing, and elevation, and for a sensor only measuring range and bearing. Since the estimation of the angular biases is decoupled from the estimation of the range bias, the simulation results for the angular biases obtained for a tracking sensor measuring range, bearing, and elevation will be the same as for a sensor only measuring bearing and elevation and having the same accuracies for the bearing and elevation measurements as the sensor measuring range, bearing, and elevation. Similarly, the simulation results for the angular biases obtained for a tracking sensor only measuring range and bearing will be the same as for a sensor only measuring bearing and having the same accuracy for the bearing measurements as the sensor measuring range and bearing. Thus, the alignment algorithm has been simulated for the four most common types of tracking sensors providing positional data.

The simulated alignment algorithm processed the measurements reported by the sensor rather than track-level data. Various targets, each having a different trajectory, were used in the bias estimation module. This was done to determine the effect of a trajectory in estimating the biases. The bias estimates from the bias estimation module were input to the bias correction module to align the measurements reported by the sensor. A trajectory which was different from any of

those used to estimate the biases was used in the bias correction module. This was done to determine how well the biases could be removed from a track's data when a different track was used to generate the bias estimates. The bias corrections were performed in real time; that is, as bias estimates were generated at each time point, they were then used to align the measurements reported by the sensor at that same instant of time.

The alignment algorithm was tested using Monte Carlo simulations, where each simulation consisted of 500 experiments. Various trajectories were used to test the algorithm. The trajectory for the first target is illustrated in Figure 4-1(a). This target is flying along a circular arc (i.e., the solid line in Figure 4-1(a)) at a constant speed of 20 m/s and at a constant altitude of 2 km. The radius of the circle along which it is moving is 10 km. The trajectory for the second target is illustrated in Figure 4-1(b). This target is flying along a straight line at a constant speed of 20 m/s and at a constant altitude of 2 km. The trajectory for the third target is illustrated in Figure 4-1(c). This target is jinking and flying at a constant altitude of 2 km. It is moving with an average speed of 22 m/s; its speed has a sinusoidal variation with a period of approximately 150 s, a minimum speed of 11 m/s, and a maximum speed of 33 m/s. Each of these targets was used in the bias estimation module to determine the values of the biases. The speeds of these targets were deliberately chosen to be small (i.e., about 20 m/s) because it is envisioned that the target used in absolute alignment would be an Unmanned Aerial Vehicle (UAV) or a helicopter. A trajectory which was different from any of those for the previous three targets was used in the bias correction module. The trajectory used in the bias correction module is illustrated in Figure 4-1(d). This target is flying along an approximate parabolic trajectory at a constant speed of 100 m/s and at a constant altitude of 2 km.

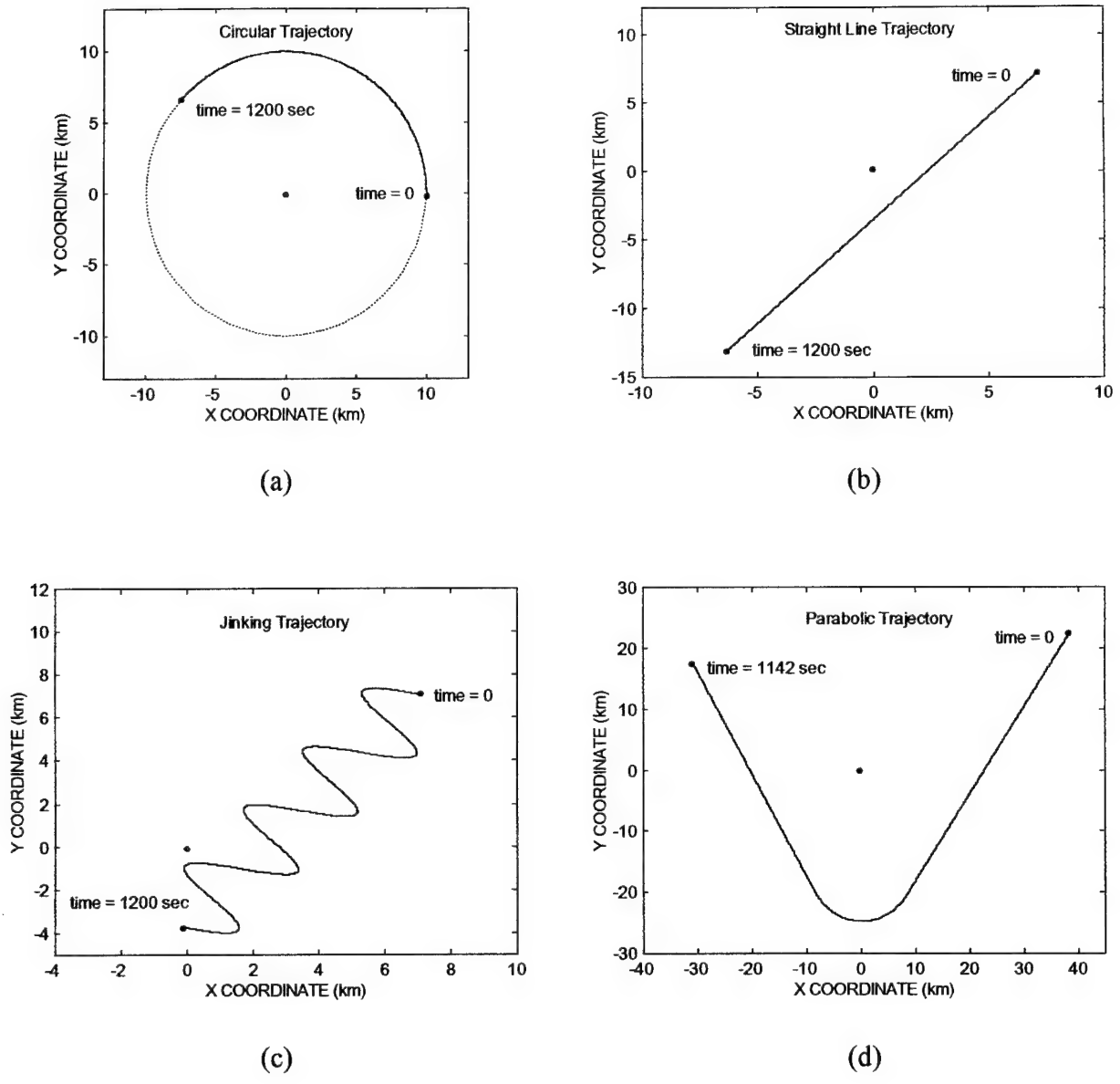

FIGURE 4-1. TARGET TRAJECTORIES USED IN THE SIMULATIONS:
(a) CIRCULAR, (b) STRAIGHT LINE, (c) JINKING, AND
(d) PARABOLIC

The sensor is located at the origin (i.e., x = y = 0 km) in all of the illustrations in Figure 4-1. Note that the sensor has no translational motion. However, two different rotational motions were simulated for the sensor. In the first set of tests, the simulated orientation of the sensor was given by attitude angles that were zero and did not change with time; that is,

$$p(t) = r(t) = y(t) = 0 \tag{4-1}$$

The attitude measurements were generated by including bias errors and random errors in the attitude angles of Equation (4-1). This case will be referred to as the "static attitude" case. In shipboard applications, a sensor may have a larger attitude than indicated in Equation (4-1) and the attitude may change with time. Thus, for the next set of tests, the simulated orientation of the sensor was given by

$$p(t) = A\cos\left(\frac{2\pi t}{T_{att}}\right) \qquad r(t) = A\cos\left(\frac{2\pi t}{T_{att}} + \frac{\pi}{4}\right) \qquad y(t) = A\sin\left(\frac{2\pi t}{T_{att}}\right) \tag{4-2}$$

where the amplitude A and period T_{att} were given by

$$A = 0.1745 \text{ rads} \qquad T_{att} = 30 \text{ s} \tag{4-3}$$

Again, the attitude measurements were generated by including bias errors and random errors in the attitude angles of Equation (4-2). This will be referred to as the "dynamic attitude" case.

4.2 SENSOR MEASURING RANGE, BEARING, AND ELEVATION

The tracking sensor provided position measurements at a periodic rate of 1 s. The measurements contained zero-mean white Gaussian random errors with the following standard deviations:

$$\sigma_{R_U} = 30 \text{ m} \qquad \sigma_{B_U} = \sigma_{E_U} = 2 \text{ millirads} \tag{4-4}$$

where σ_{B_U} and σ_{E_U} are the standard deviations for the random errors in the bearing and elevation, respectively, and σ_{R_U} is the standard deviation for the random error in the range. The random

errors in the range, bearing, and elevation were mutually uncorrelated. The following constant bias offsets were included in the range, bearing, and elevation measurements:

$$R_{bias} = 25 \text{ m} \qquad B_{bias} = 15 \text{ millirads} \qquad E_{bias} = 10 \text{ millirads} \tag{4-5}$$

A system reporting the attitude of the sensor was simulated to provide the pitch, roll, and yaw angles at a periodic rate of 1 s. The pitch, roll, and yaw angles contained zero-mean white Gaussian random errors with the following standard deviations:

$$\sigma_p = \sigma_r = \sigma_y = 0.1 \text{ millirads} \tag{4-6}$$

where σ_p, σ_r, and σ_y are the standard deviations for the random errors in the pitch, roll, and yaw angles, respectively. The random errors in the pitch, roll, and yaw angles were mutually uncorrelated. The following constant bias offsets were included in the pitch, roll, and yaw angles:

$$p_{bias} = 5 \text{ millirads} \qquad r_{bias} = y_{bias} = -5 \text{ millirads} \tag{4-7}$$

The absolute standard was simulated to provide precise location information at a periodic rate of 1 s for both the sensor and the targets used in the bias estimation module. The (rectangular) position vectors giving the locations were expressed in the (true) stabilized frame located at the true position of the sensor, which had no translational motion. The x, y, and z components of the position vectors reported by the absolute standard contained zero-mean white Gaussian random errors with the following standard deviations:

$$\sigma_x^{std} = \sigma_y^{std} = \sigma_z^{std} = 10 \text{ m} \tag{4-8}$$

where σ_x^{std}, σ_y^{std}, and σ_z^{std} are the standard deviations for the random errors in the x, y, and z

components, respectively. The random errors in the x, y, and z components were uncorrelated. No bias errors were included in the position vectors reported by the absolute standard.

The filters in the bias estimation module require dynamical models that describe how the biases change with time. Linear dynamical models were used for both the range bias and the angular biases. A constant velocity model was used for the range bias dynamics and a constant model was used for the dynamics of the angular biases. Specifically, these dynamical models were given by

$$\begin{bmatrix} R_{bias}(t_k) \\ \dot{R}_{bias}(t_k) \end{bmatrix} = \begin{bmatrix} 1 & T \\ 0 & 1 \end{bmatrix} \begin{bmatrix} R_{bias}(t_{k-1}) \\ \dot{R}_{bias}(t_{k-1}) \end{bmatrix} + \boldsymbol{W}_R(t_{k-1}) \tag{4-9}$$

and

$$\boldsymbol{b}_{ang}(t_k) = \boldsymbol{b}_{ang}(t_{k-1}) + \boldsymbol{W}_{ang}(t_{k-1}) \tag{4-10}$$

where $\dot{R}_{bias}$ is the time rate of change of the range bias, $T = t_k - t_{k-1}$ is the sampling period (T = 1 s in the simulations), $\boldsymbol{b}_{ang} = \begin{bmatrix} A_{bias} & E_{bias} & p_{bias} & r_{bias} \end{bmatrix}^T$ is the vector containing the angular biases, $\boldsymbol{W}_R$ is the process noise vector for range bias dynamics, and $\boldsymbol{W}_{ang}$ is the process noise vector for the angular bias dynamics. These process noise terms were assumed to be zero-mean white Gaussian processes with the following covariances:

$$cov[\boldsymbol{W}_R(t_{k-1})] = q_R^2 \begin{bmatrix} T^3/3 & T^2/2 \\ T^2/2 & T \end{bmatrix} \qquad cov[\boldsymbol{W}_{ang}(t_{k-1})] = q_{ang}^2 T^2 I_4 \tag{4-11}$$

where cov is the covariance operator and I_4 is the 4 x 4 identity matrix. The values of q_R and q_{ang} were given by

$$q_R = 0.01 \text{ m/s}^{1.5} \qquad q_{ang} = 1 \text{ microrad/s} \tag{4-12}$$

Linear Kalman filters were used to estimate both the range bias and the angular biases. The first data point for the target reported by the sensor was used to compute the initial range bias estimate and the first two data points were used to compute the initial range bias rate estimate. Subsequent range bias and range bias rate estimates were generated by the Kalman filter for the range bias. The initial estimates used in the Kalman filter for the angular biases were generated by a least-squares estimator that processed the first fifty data points for the target. Fewer data points could have been used to initialize the filter for the angular biases; however, this usually resulted in very noisy estimates. Since the computation of the initial estimates for the angular biases used the first fifty data points, the initial estimates of the angular biases were produced only after 50 s of data had been reported by the sensor for the target. Thus, the application of the estimated angular biases in the bias correction module occurred only after 50 s of data (i.e., fifty data points) had been processed in the bias estimation module. In contrast, the application of the estimated range bias in the bias correction module occurred after one data point had been processed in the bias estimation module.

The results for the static attitude case will be presented first. The range bias results are shown in Figure 4-2. The range bias estimates for the circular trajectory appear in Figure 4-2(a). The range bias estimates are denoted by the solid line, which represents the average over the 500 experiments. The true value of the range bias is represented by the dashed line. The estimates

for the straight line and jinking trajectories are not presented because they are nearly identical to those for the circular trajectory. The root-mean-square-error (RMSE) in the estimated range bias is presented in Figure 4-2(b). The circles are the results for the circular trajectory, the plus-marks for the straight line trajectory, and the stars for the jinking trajectory. The RMSE in the estimate of a quantity x at time t is computed by

$$\text{RMSE in the estimate of x at time } t = \sqrt{\frac{1}{N}\sum_{i=1}^{N}\left[x^{true}(t) - \hat{x}_i(t)\right]^2} \qquad (4\text{-}13)$$

where $x^{true}(t)$ is the true value of x at time t, $\hat{x}_i(t)$ is the estimated value of x in the i^{th} experiment at time t, and N is the number of experiments in the simulation ($N = 500$). The estimate of the range bias converges quickly to its true value. The RMSE indicates that the steady-state accuracy of the range bias is approximately 5 m, which is comparable to the standard deviation output by the range bias filter.

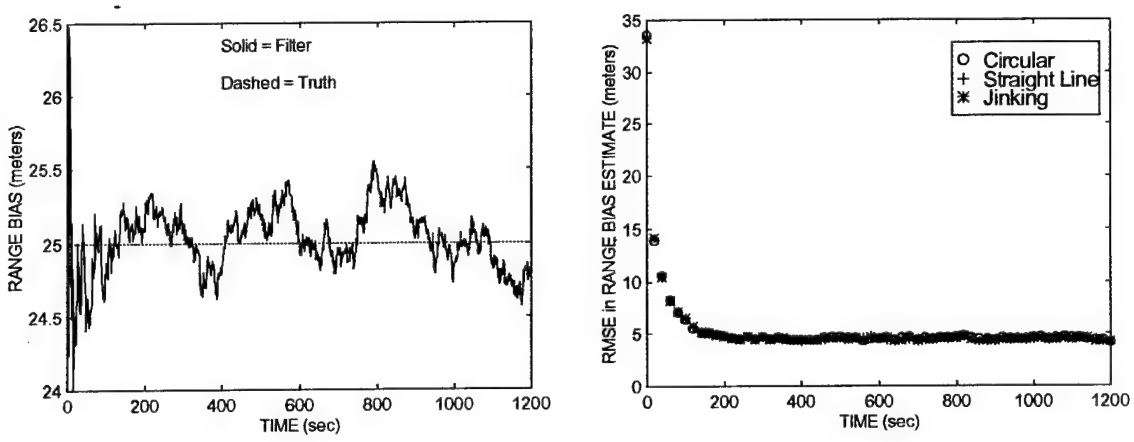

(a) (b)

FIGURE 4-2. RANGE BIAS FILTER RESULTS FOR THE STATIC ATTITUDE CASE: (a) ESTIMATES AND (b) RMSEs

The estimates of the angular biases appear in Figure 4-3. The results for the circular trajectory are shown in (a), the straight line trajectory in (b), and the jinking trajectory in (c). Again the estimates are denoted by the solid lines, which represent the averages over the 500 experiments, and the dashed lines denote the true values of the biases. For the circular and jinking trajectories, the azimuth bias quickly converges to its true value, but it takes about 300 s to converge for the straight line trajectory. The estimates of the remaining angular biases take much longer to converge, about 400 to 500 s.† Note that the estimates of the angular biases contain much error in the first 400 s for the straight line trajectory; much larger than is observed for the circular or jinking trajectories.‡

The RMSEs in the estimates of the angular biases are presented in Figure 4-4. The circles are the RMSEs for the circular trajectory, the plus-marks for the straight line trajectory, and the stars for the jinking trajectory. Although the RMSEs for the straight line trajectory are initially an order of magnitude larger than those for the other two trajectories, they eventually settle down to values close to or smaller than the ones for the other two trajectories; after 400 s, the RMSEs in the elevation, pitch, and roll biases for the straight line trajectory are smaller than the RMSEs for the other two trajectories for much of the time. Most of the angular biases can be determined to accuracies of 1 millirad in 500 to 600 s, and to accuracies of 0.1 to 0.3 millirads at 1200 s. These RMSEs for the angular biases are comparable to the standard deviations output by the filter for the angular biases.

† This is the reason that a constant model rather than a constant velocity model was used for the dynamics of the angular biases in these simulations. Several tests were performed with a constant velocity model and time-varying biases, but the convergence of the angular biases and their rates took several thousands of seconds.

‡ This probably is caused by the smaller displacement in the bearing that initially occurs for the straight line trajectory compared to the circular or jinking trajectories. As the straight line trajectory approaches the sensor, the displacement for the bearing increases (eventually larger than for the circular and jinking trajectories) and the estimation accuracy of the angular biases improves.

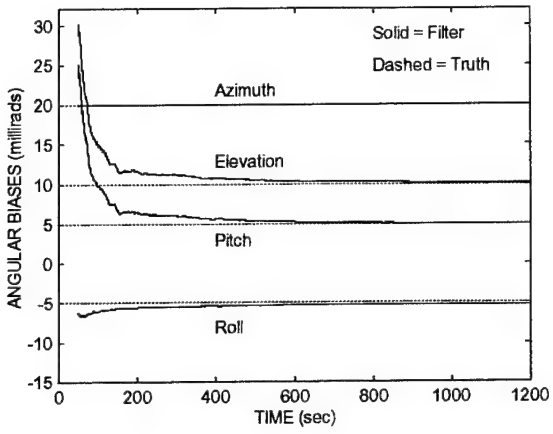

(a)

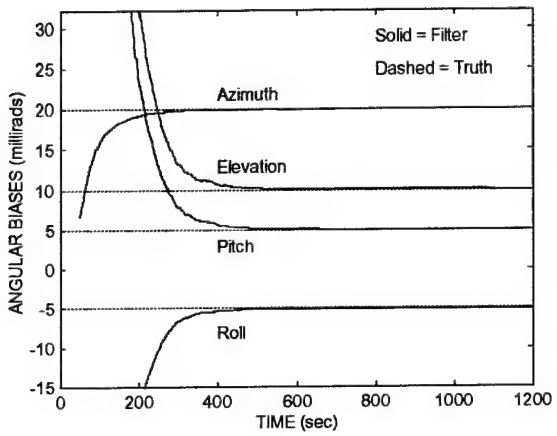

(b)

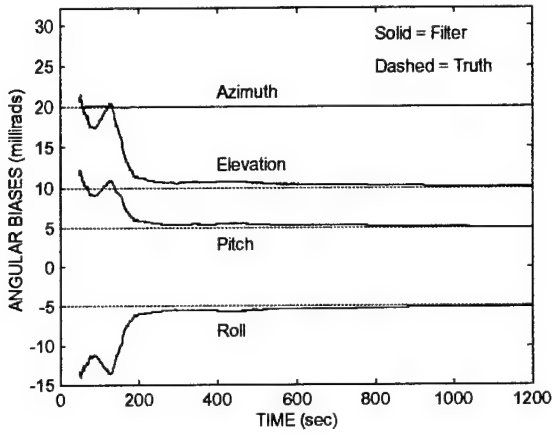

(c)

FIGURE 4-3. ESTIMATES OF THE ANGULAR BIASES FOR THE STATIC ATTITUDE CASE: (a) CIRCULAR, (b) STRAIGHT LINE, AND (c) JINKING TRAJECTORIES

The bias estimates were input to the bias correction module to remove the biases from the stabilized measurements reported by the sensor for the parabolic trajectory. The results are presented in Figure 4-5. The unaligned and aligned RMSEs for the range are presented in (a), the unaligned and aligned RMSEs for the bearing in (b), and the unaligned and aligned RMSEs for the elevation in (c). Here, "unaligned" refers to the case where the biases have not been removed

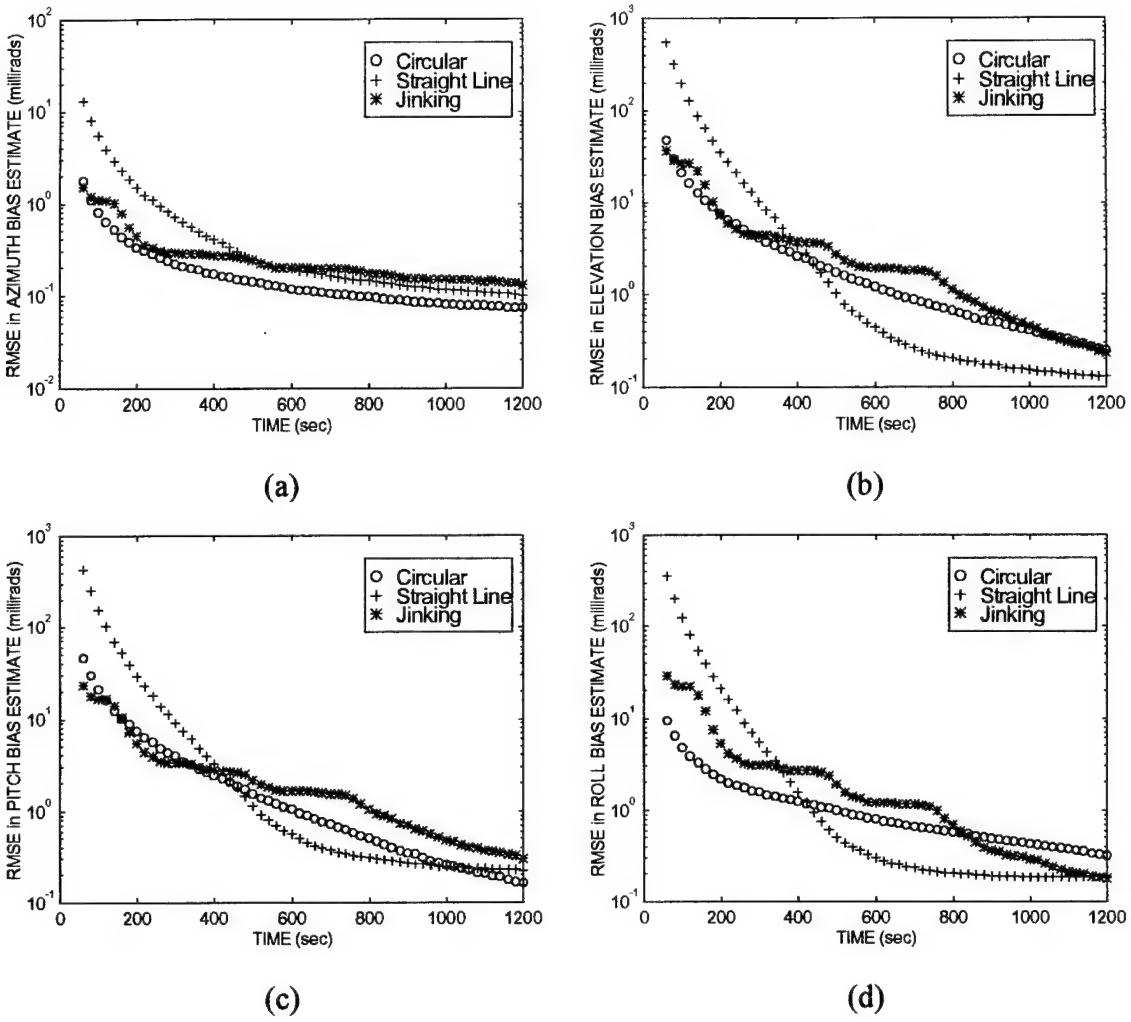

FIGURE 4-4. RMSEs IN THE ESTIMATES OF THE ANGULAR BIASES FOR THE STATIC ATTITUDE CASE: (a) AZIMUTH, (b) ELEVATION, (c) PITCH, AND (d) ROLL BIASES

from the stabilized measurements for the parabolic trajectory, while "aligned" refers to the case where the biases have been removed from the stabilized measurements in the bias correction module using the estimated biases. The circles are the aligned RMSEs when the circular trajectory is used to estimate the biases, the plus-marks are the aligned RMSEs for the straight line trajectory, the stars are the aligned RMSEs for the jinking trajectory, the solid lines are the unaligned RMSEs in the stabilized coordinates, and the dashed lines represent the values of the standard

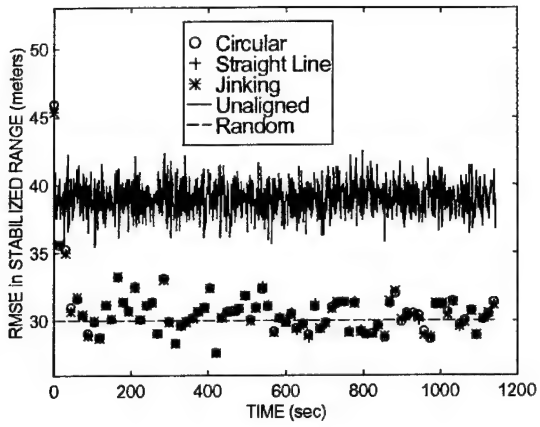

(a)

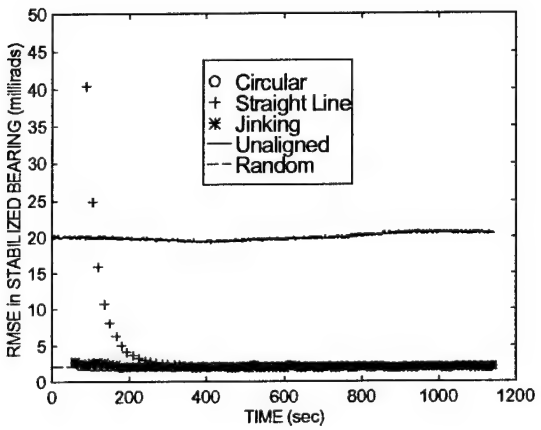

(b)

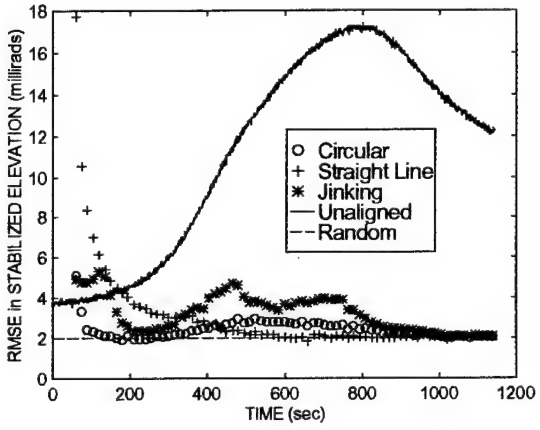

(c)

FIGURE 4-5. UNALIGNED AND ALIGNED ERRORS FOR THE PARABOLIC TRAJECTORY AND THE STATIC ATTITUDE CASE: (a) RANGE, (b) BEARING, AND (c) ELEVATION

deviations in the stabilized coordinates due only to the random error. The unaligned and aligned RMSEs for a quantity x at time t are computed by

$$\text{Unaligned RMSE at time } t = \sqrt{\frac{1}{N}\sum_{i=1}^{N}\left[x^{true}(t) - x_i^{unaligned}(t)\right]^2} \qquad (4\text{-}14)$$

and

$$\text{Aligned RMSE at time } t = \sqrt{\frac{1}{N}\sum_{i=1}^{N}\left[x^{true}(t) - x_i^{aligned}(t)\right]^2} \tag{4-15}$$

where $x^{true}(t)$ is the true value of x at time t, $x_i^{unaligned}(t)$ is the unaligned value of x in the i^{th} experiment at time t, $x_i^{aligned}(t)$ is the aligned value of x in the i^{th} experiment at time t, and N is the number of experiments in the simulation ($N = 500$).

Since the range bias is 25 m and the standard deviation for the random range error is 30 m, the total error in the range should be 39 m (i.e., $\sqrt{(25\text{ m})^2 + (30\text{ m})^2}$). The average value of the unaligned RMSE in the range for the parabolic trajectory is consistent with this value. The aligned RMSEs in the range for the parabolic trajectory are nearly the same when any of the three trajectories is used to estimate the biases. Since the range bias can be estimated to an accuracy of about 5 m, the total error in the range after alignment should be about 30.4 m (i.e., $\sqrt{(5\text{ m})^2 + (30\text{ m})^2}$). The average values of the aligned RMSEs in the range are consistent with this value. The dashed line in Figure 4-5(a) represents the value of the standard deviation in the range due only to the random errors, which has a value of 30 m.

The unaligned RMSE in the stabilized bearing for the parabolic trajectory in Figure 4-5(b) is about 20 millirads. This error is caused by the bias errors in the bearing, elevation, pitch, roll, and yaw angles, as well as the random errors in these angles. Equation (3-37) can be used to approximately determine the contribution of the biases to the error in the stabilized bearing for this case. When the circular and jinking trajectories are used to estimate the biases, the stabilized bearing for the parabolic trajectory can be accurately aligned over the entire time interval. However, when

the straight line trajectory is used to estimate the biases, the error in the aligned bearing for the parabolic trajectory is initially much larger than for the unaligned bearing. This occurs because of the large amount of estimation error in the initial angular bias estimates for the straight line trajectory. Thus, the performance is initially degraded by correcting the stabilized bearing when the straight line trajectory is used to estimate the biases; that is, it is better to use the unaligned bearing for the first 100 to 150 s when the straight line trajectory is used to estimate the biases.

The variation of the unaligned RMSE in the stabilized elevation for the parabolic trajectory in Figure 4-5(c) is quite pronounced; it varies from a minimum of about 4 millirads to a maximum of about 17 millirads. Equation (3-38) can be used to approximately determine the contribution of the biases to the error in the stabilized elevation for this case. Based on Equation (3-38), the unaligned RMSE for the elevation due to the biases has a minimum value of about 3 millirads at a bearing of 45 deg; it then increases quickly as the bearing increases and achieves a maximum value of about 17 millirads at a bearing of 225 deg; and then it decreases as the bearing increases. The bearing of the parabolic trajectory has a value of 45 deg near the time at which the minimum RMSE in Figure 4-5(c) occurs; the bearing of the parabolic trajectory then increases and the RMSE is observed to increase quickly; the bearing of the parabolic trajectory has a value of 225 deg near the time at which the maximum RMSE in Figure 4-5(c) occurs; and then the RMSE in Figure 4-5(c) decreases as the bearing increases. Thus, the shape of the parabolic trajectory explains the variation in the unaligned RMSE for the elevation. The aligned RMSEs indicate that it takes about 100 to 150 s to accurately align the elevation. This occurs because it takes a long time for the elevation, pitch, and roll bias estimates to converge, and it is these three bias estimates that make the major contribution in removing the bias errors in the elevation. Similar to the bearing, the error in the aligned elevation is initially much larger than the unaligned elevation when the straight line trajectory is used to estimate the biases.

Note that there is an increase in the error for the aligned elevation between 400 and 800 s when the circular or jinking trajectories are used to estimate the biases. This is due to the estimation error in the biases and the shape of the parabolic trajectory. Compared to the circular and jinking trajectories, this increase is not as significant when the straight line trajectory is used to estimate the biases; the reason is that the errors in the estimates of the elevation, pitch, and roll bias estimates are usually much smaller between 400 and 800 s for the straight line trajectory compared to the circular and jinking trajectories (see Figure 4-4). The increase is most pronounced for the jinking trajectory because the errors in the estimates are generally largest for the jinking trajectory in this time interval.

The results for the dynamic attitude case will be presented next. The results for the range bias filter are not shown because they are nearly identical to those presented in Figure 4-2 for the static attitude case. The estimates of the angular biases appear in Figure 4-6. The results for the circular trajectory are shown in (a), the straight line trajectory in (b), and the jinking trajectory in (c). Note that the initial estimates of the angular biases for the straight line trajectory are more accurate than for the static attitude case (see Figure 4-3(b)). This is probably the result of larger displacements in the bearing and elevation that occur because of the larger attitude variations for the dynamic attitude case. Also, the initial estimates of the elevation, pitch, and roll biases for the circular and jinking trajectories usually contain less error than for the static attitude case. However, for all of the trajectories, it appears to take slightly longer for the bias estimates to converge to their true values than for the static attitude case.

The RMSEs in the estimates of the angular biases are presented in Figure 4-7. The results are similar to the results obtained for the static attitude case, except that the initial RMSEs are much smaller for the dynamic attitude case. This is particularly true for the straight line trajectory (see Figure 4-4). Most of the angular biases can be determined to accuracies of 1 millirad in 300 to

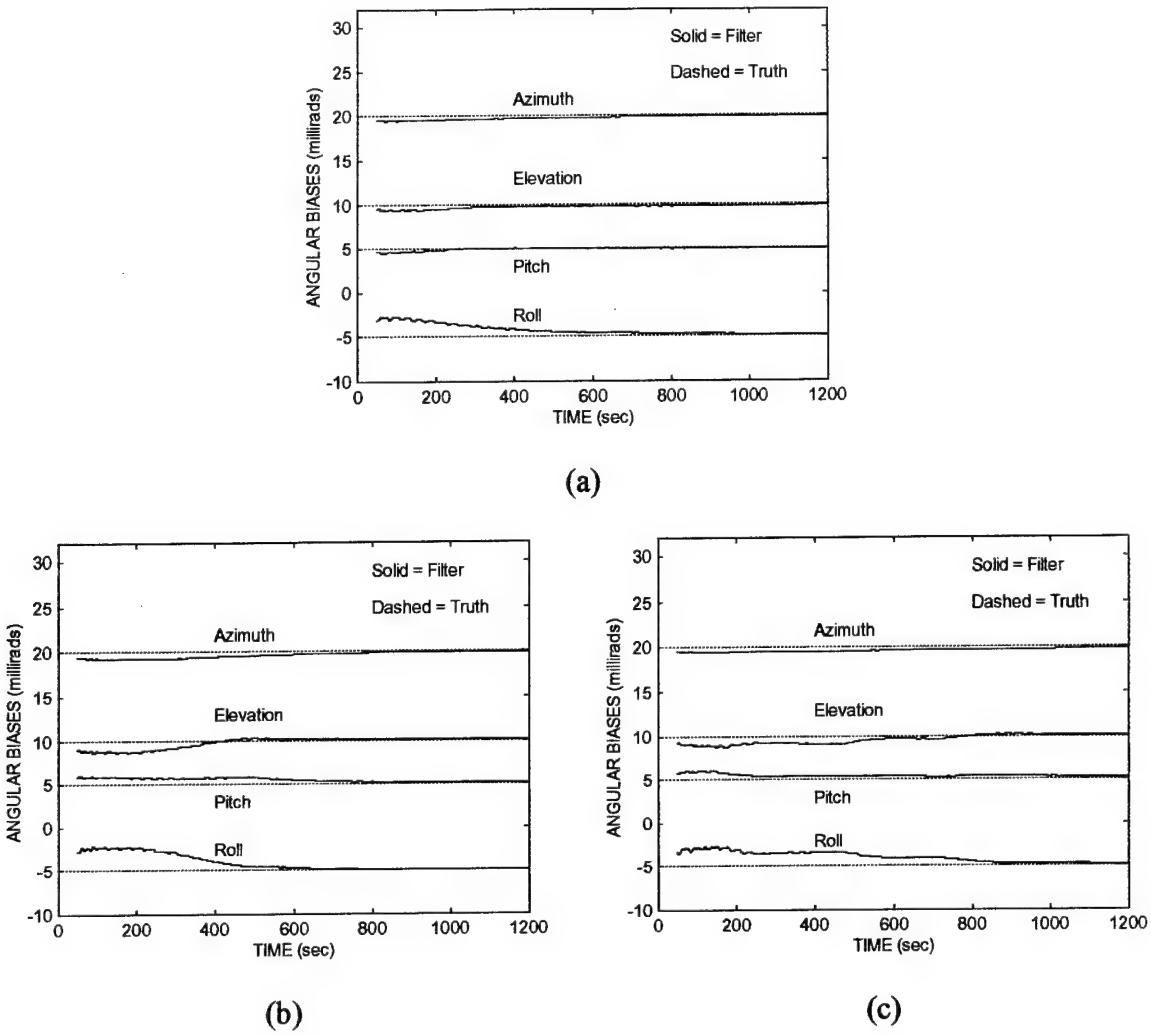

FIGURE 4-6. ESTIMATES OF THE ANGULAR BIASES FOR THE DYNAMIC ATTITUDE CASE: (a) CIRCULAR, (b) STRAIGHT LINE, AND (c) JINKING TRAJECTORIES

400 s, which is faster than for the static attitude case, and to accuracies of 0.1 to 0.3 millirads at 1200 s, which is about the same as for the static attitude case.

The bias estimates were input to the bias correction module to remove the biases from the stabilized measurements reported by the sensor for the parabolic trajectory. The results are presented in Figure 4-8. The unaligned and aligned RMSEs for the bearing are presented in (a), and the unaligned and aligned RMSEs for the elevation in (b). The unaligned and aligned RMSEs for

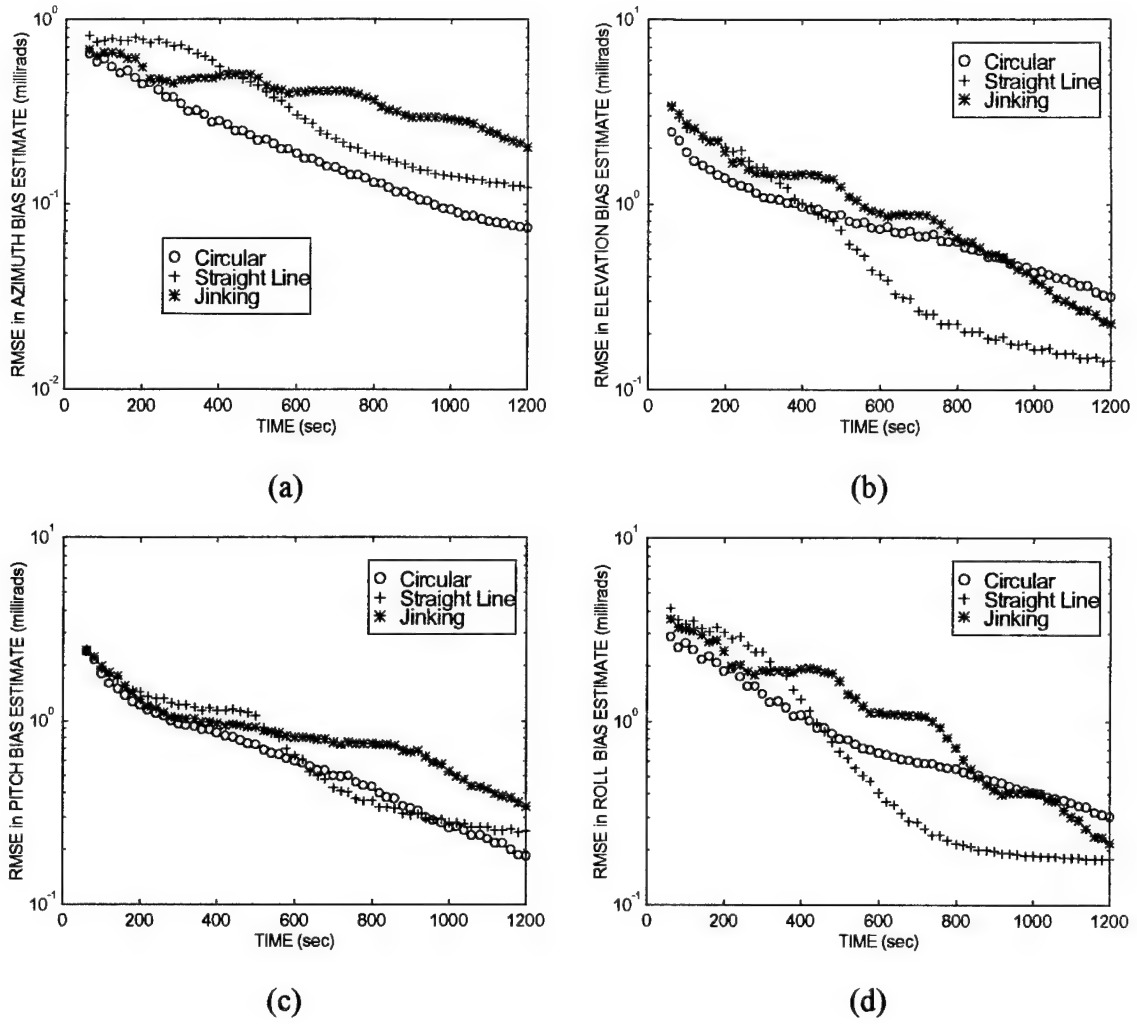

FIGURE 4-7. RMSEs IN THE ESTIMATES OF THE ANGULAR BIASES FOR THE DYNAMIC ATTITUDE CASE: (a) AZIMUTH, (b) ELEVATION, (c) PITCH, AND (d) ROLL BIASES

the range are not presented because they are nearly identical to those presented in Figure 4-5(a) for the static attitude case. Note the large oscillatory variations in the unaligned RMSEs in the stabilized bearing and elevation. Although the bearing and elevation are stabilized using the measured attitude angles, the uncompensated bias errors along with the sinusoidal variation in the attitude angles cause this oscillatory variation in the (unaligned) stabilized bearing and elevation. The stabilized bearing for the parabolic trajectory can be accurately aligned over the entire time interval and this does not depend on the trajectory used to estimate the biases; the oscillatory variation

has also been removed from the stabilized bearing after alignment. The stabilized elevation for the parabolic trajectory can also be accurately aligned. Again, there is a slight increase in the error in the aligned elevation between 400 and 800 s when the circular and jinking trajectories are used to estimate the biases. However, this increase in less pronounced in the dynamic attitude case, which is due to the more accurate bias estimates between 400 and 800 s compared to the static attitude case. Note that the results for both the bearing and elevation are much better in the first 200 s for the straight line trajectory than was obtained for static attitude case (see Figure 4-5); this is due to the much more accurate initial bias estimates for the straight line trajectory in the dynamic attitude case.

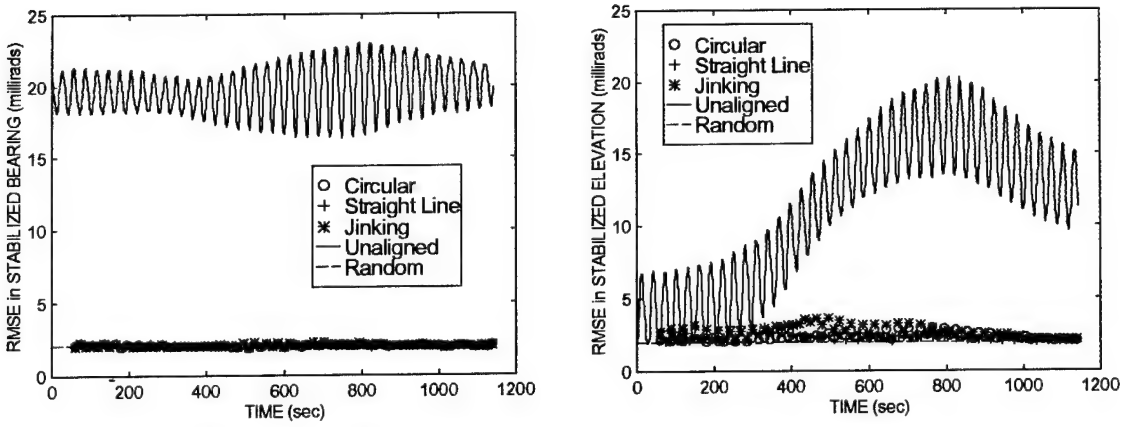

(a) (b)

FIGURE 4-8. UNALIGNED AND ALIGNED ERRORS FOR THE PARABOLIC TRAJECTORY AND THE DYNAMIC ATTITUDE CASE: (a) BEARING AND (b) ELEVATION

All of the previous results were based on an absolute standard that had the accuracies presented in equation (4-8), which represents a total position accuracy of about 17 m. Since the accuracy of the absolute standard may be different (e.g., GPS has different accuracies depending on its mode of operation), it is instructive to determine the effect of the accuracy for the absolute

standard on the alignment accuracy. Thus, another set of simulations were performed for the circular trajectory and for the static attitude case. Each simulation consisted of 500 experiments. The same values of the parameters presented in Equations (4-4) to (4-7) were used; however, the total positional standard deviation in the absolute standard was varied. Three different values of the total positional standard deviation in the absolute standard were used: 1 m, 30 m, and 100 m.

The accuracies (i.e., RMSEs) of the bias estimates are presented in Figure 4-9 for the three different positional standard deviations in the absolute standard. The circles are the results for a total positional standard deviation of 1 m, the plus-marks for 30 m, and the stars for 100 m. As expected, the accuracies are best for a positional standard deviation of 1 m, followed by 30 m, and then by 100 m. The RMSEs in the range bias estimates for the 30 m standard are about 20% larger than the RMSEs for the 1 m standard, and the RMSEs in the range bias estimate for the 100 m standard are about 130% larger than the RMSEs for the 1 m standard. For the estimates of the angular biases, the RMSEs for the 30 m standard are about 50% larger than the RMSEs for the 1 m standard, and the RMSEs for the 100 m standard are about 300% larger than the RMSEs for the 1 m standard.

The bias estimates were input to the bias correction module to remove the biases from the stabilized measurements reported by the sensor for the parabolic trajectory. The results are presented in Figure 4-10 for the three different positional standard deviations in the absolute standard. The RMSEs for the stabilized range are presented in (a), the RMSEs for the stabilized bearing in (b), and the RMSEs for the stabilized elevation in (c). The x-marks represent the RMSEs in the unaligned coordinates, the solid lines represent the standard deviations due only to the random errors, the circles represent the RMSEs in the aligned coordinates for the 1 m standard, the plus-marks represent the RMSEs in the aligned coordinates for the 30 m standard, and the stars represent the RMSEs in the aligned coordinates for the 100 m standard. Clearly, the alignment accuracy is best for a positional standard deviation of 1 m, followed closely by 30 m,

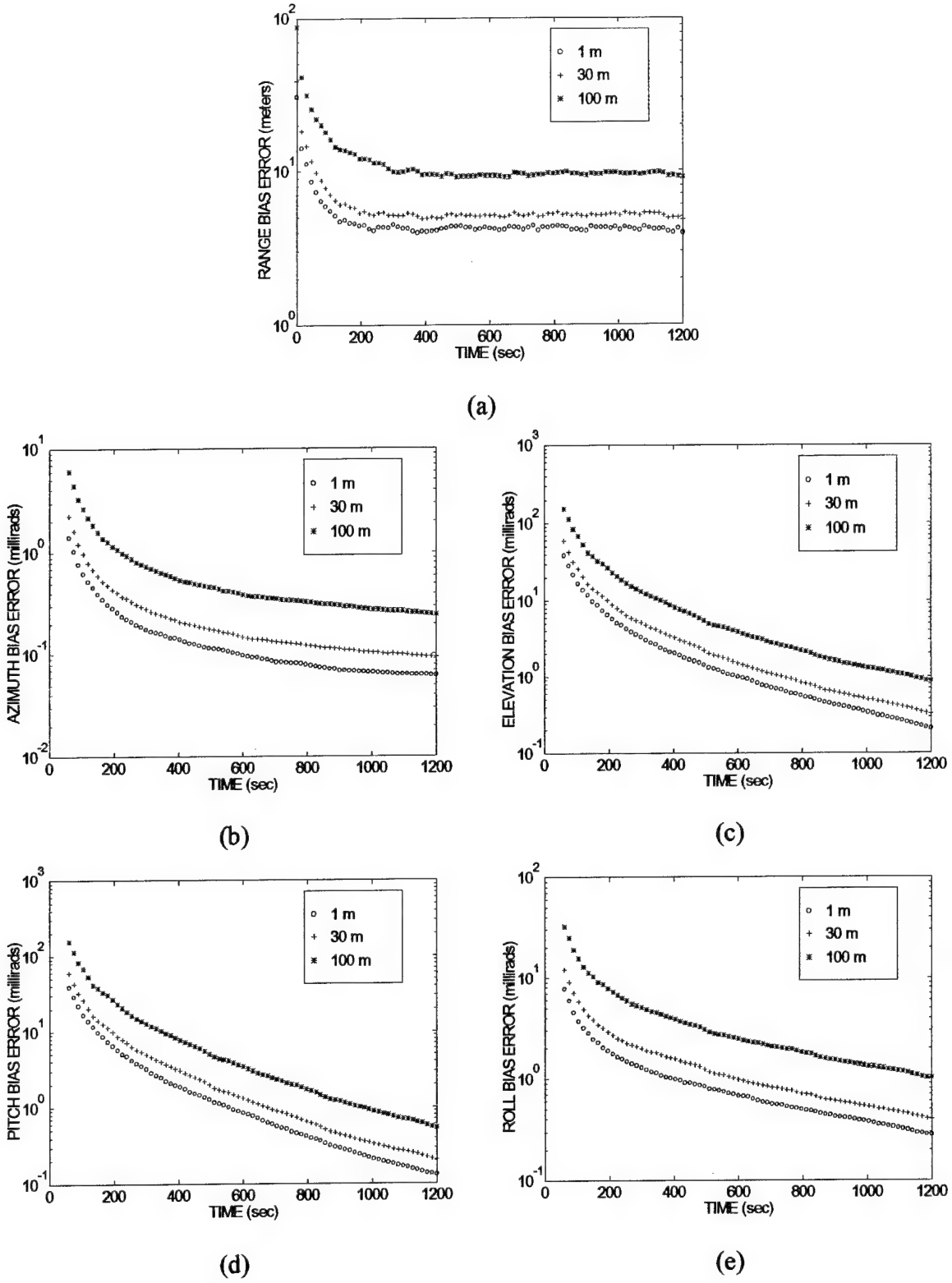

FIGURE 4-9. RMSEs IN THE FILTERED BIAS ESTIMATES FOR THREE DIFFERENT POSITIONAL ACCURACIES IN THE ABSOLUTE STANDARD: CIRCULAR TRAJECTORY AND STATIC ATTITUDE CASE

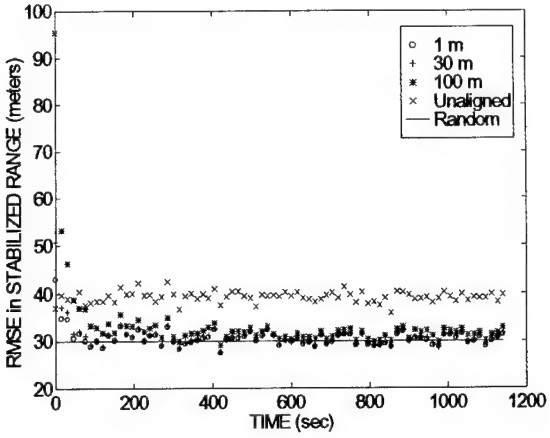

(a)

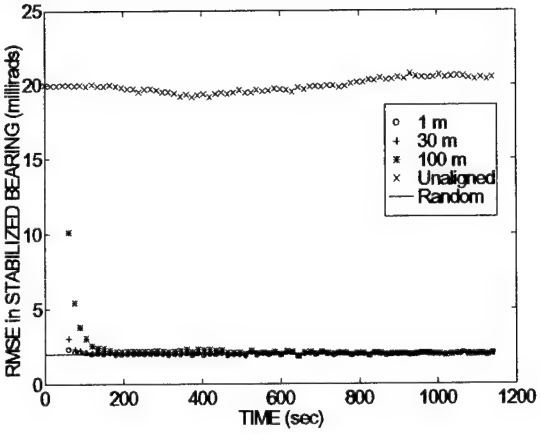

(b)

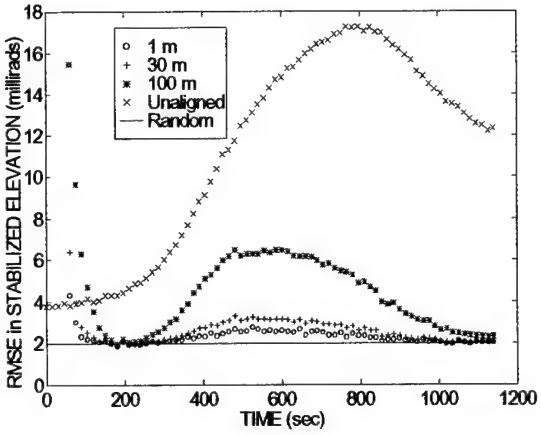

(c)

FIGURE 4-10. UNALIGNED AND ALIGNED ERRORS FOR THE PARABOLIC TRAJECTORY FOR THREE DIFFERENT POSITIONAL ACCURACIES IN THE ABSOLUTE STANDARD: CIRCULAR TRAJECTORY USED TO ESTIMATE THE BIASES AND STATIC ATTITUDE CASE

and then by 100 m. However, it should be noted that the alignment accuracies for the stabilized bearing are nearly the same for all three of the positional standard deviations after about 100 to 150 s. Also, the 30 m standard produces nearly the same alignment as the 1 m standard for the stabilized elevation and the stabilized range. The quality of the alignment for the 100 m standard is poorer for the stabilized elevation than those of the 1 m and 30 m standards; the same is true for

the stabilized range. Thus, marginal gains in the overall alignment quality are obtained in going from a 30 m standard to a 1 m standard. However, larger gains are obtained in going from a 100 m standard to either a 30 m or 1 m standard. To illustrate this, the average values of the unaligned and aligned RMSEs in the stabilized coordinates from 200 to 1142 s are presented in Table 4-1. This time interval was chosen so as to minimize the effects of the initial errors in the bias estimates. The 30 m standard gives about 98% of the average alignment performance of the 1 m standard. The 100 m standard gives 99% of the average alignment performance of the 1 m standard for the stabilized bearing, but only about 85% of the performance for the stabilized range and stabilized elevation.

TABLE 4-1. AVERAGE RMSEs FOR THE UNALIGNED COORDINATES AND THE ALIGNED COORDINATES IN THE PARABOLIC TRAJECTORY FOR THE THREE POSITIONAL STANDARD DEVIATIONS IN THE ABSOLUTE STANDARD

	Positional Standard Deviation in the Absolute Standard			Unaligned
	1 m	30 m	100 m	
Stabilized Range	30.3 m	30.5 m	31.5 m	39.0 m
Stabilized Bearing	2.0 mrad	2.0 mrad	2.1 mrad	19.9 mrad
Stabilized Elevation	2.3 mrad	2.5 mrad	4.3 mrad	12.8 mrad

4.3 SENSOR ONLY MEASURING RANGE AND BEARING

The simulation of the tracking sensor only measuring range and bearing is the same as described for the sensor in Section 4.2 except that no elevation bias errors and no random elevation errors were included in the measurements. Also, the elevation measurement was ignored in

this case. The simulation of the system reporting the attitude of the sensor and the simulation of the absolute standard are the same as described in Section 4.2.

In the bias estimation module, some of the equations require the elevation of the target as reported by the sensor. However, the sensor provides no elevation for the target. Since the locations of the target and the sensor are reported by the absolute standard, the elevation of the target in the sensor's reference frame can be computed. This elevation, which is derived from the locations reported by the absolute standard, will be used in the bias estimation module for the target. This implies that there is no elevation bias and thus no elevation bias needs to be estimated.

The difficult problem is in the bias correction module. Since the absolute standard is only assumed to provide the location of the target used in the bias estimation module, the elevations of arbitrary targets reported by the sensor cannot be determined. In this case, the only thing that can be done is to assign an arbitrary value to the elevation. Thus, in the bias correction module, the elevation of the parabolic trajectory will assigned the value of zero, which of course is not the correct value.

Only the static attitude case was simulated. The range bias results are presented in Figure 4-11. The range bias estimates for the circular trajectory appear in Figure 4-11(a). The estimates for the straight line and jinking trajectories are not presented because they are nearly identical to those for the circular trajectory. The RMSEs in the range bias estimates for the trajectories of the three targets are presented in Figure 4-11(b). These results for the estimates and the RMSEs for the range bias are very similar to the results obtained for the sensor measuring range, bearing, and elevation. This is expected because the estimation of the range bias is decoupled from the estimation of the angular biases for both sensors.

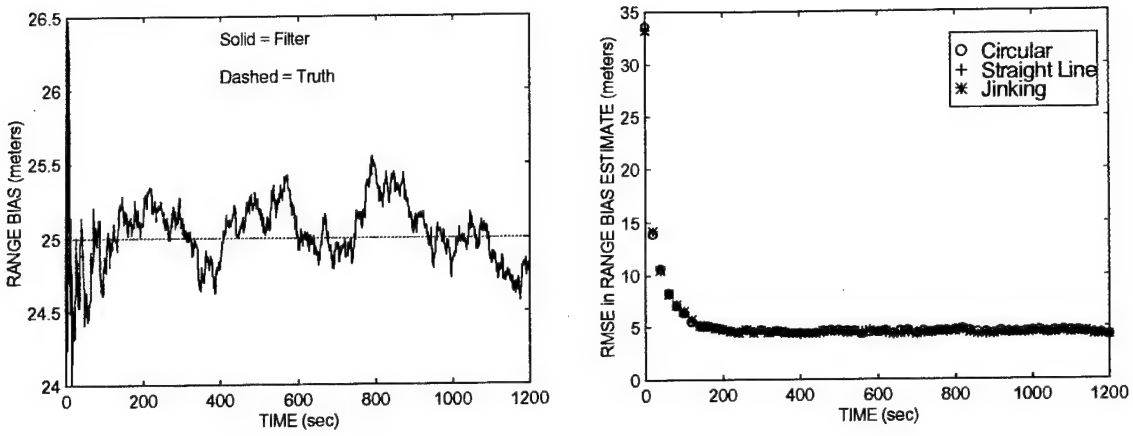

(a) (b)

FIGURE 4-11. RANGE BIAS FILTER RESULTS FOR A SENSOR ONLY MEASURING RANGE AND BEARING FOR THE STATIC ATTITUDE CASE: (a) ESTIMATES AND (b) RMSEs

The estimate of the angular biases appear in Figure 4-12. The results for the circular trajectory are shown in (a), the straight line trajectory in (b), and the jinking trajectory in (c). The estimates converge in 400 to 500 s. For the straight line and jinking trajectories, the estimates are very inaccurate in the first 300 to 400 s. For the sensor measuring range, bearing, and elevation, the initial estimates for the jinking trajectory were much more accurate (see Figure 4-3). The decrease in the accuracy of the initial estimates for the sensor only measuring range and bearing is due to having only one measurement equation (i.e., Equation (3-65)) as opposed to having two measurement equations (i.e., Equations (3-65) and (3-66)) for the sensor measuring range, bearing, and elevation.

The RMSEs in the estimates of the angular biases are presented in Figure 4-13. The circles are the RMSEs for the circular trajectory, the plus-marks for the straight line trajectory, and the stars for the jinking trajectory. The initial RMSEs are an order of magnitude larger than the

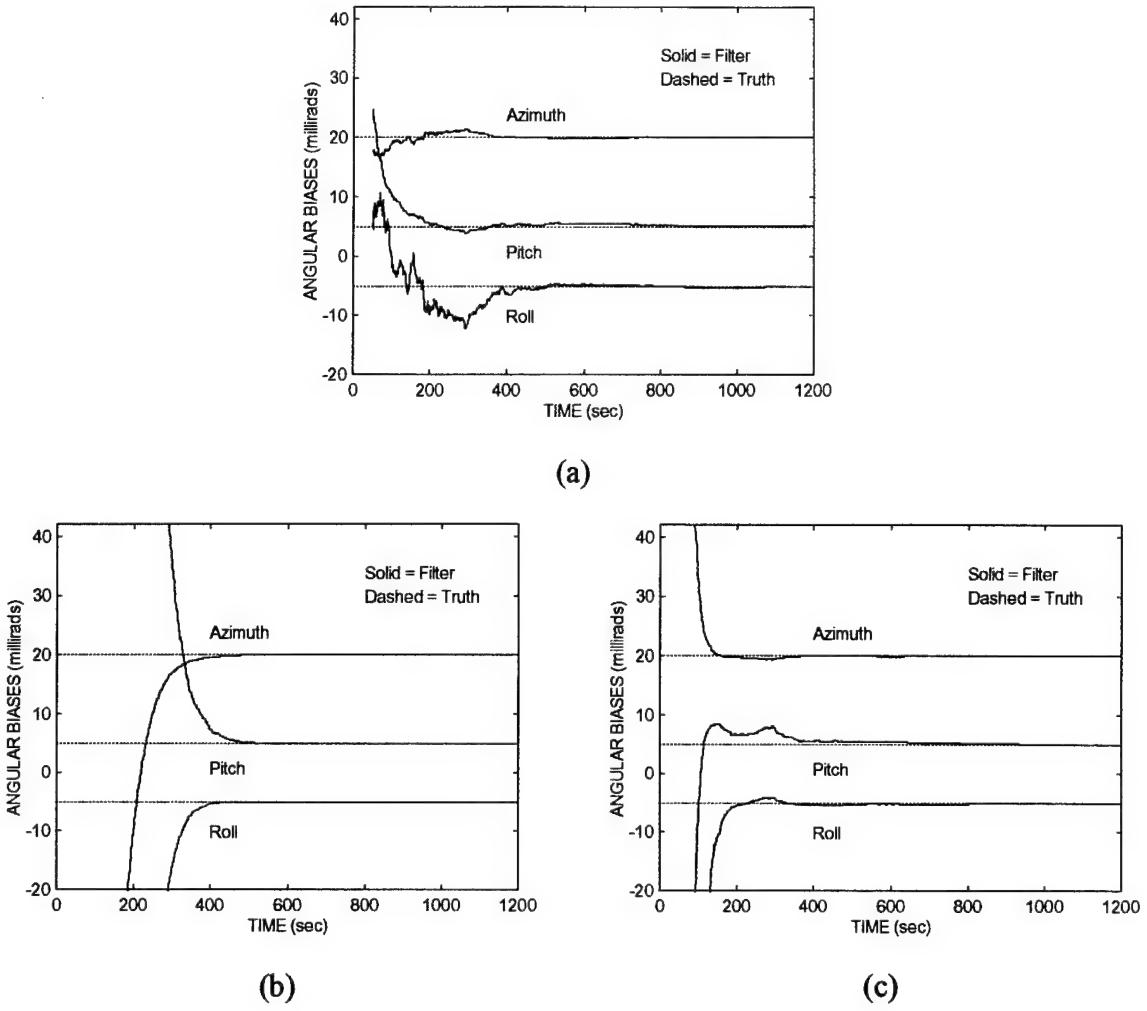

FIGURE 4-12. ESTIMATES OF THE ANGULAR BIASES FOR A SENSOR ONLY MEASURING RANGE AND BEARING FOR THE STATIC ATTITUDE CASE: (a) CIRCULAR, (b) STRAIGHT LINE, AND (c) JINKING TRAJECTORIES

corresponding RMSEs for the sensor measuring range, bearing, and elevation (see Figure 4-4). For the straight line trajectory, most of the biases can be determined to accuracies of 1 millirad in 400 to 500 s, and to accuracies of 0.1 to 0.5 millirads at 1200 s. This is comparable to the results obtained for the sensor measuring range, bearing, and elevation. The jinking trajectory takes 400 to 800 s to obtain accuracies of 1 millirad for the various biases, and accuracies of 0.2 to

0.8 millirads can be obtained at 1200 s. This is slightly worse than the performance obtained for the sensor measuring range, bearing, and elevation. For the circular trajectory, it takes 800 to 1200 s to obtain accuracies near 1 millirad for the various biases. This is considerably worse than the performance obtained for the sensor measuring range, bearing, and elevation.

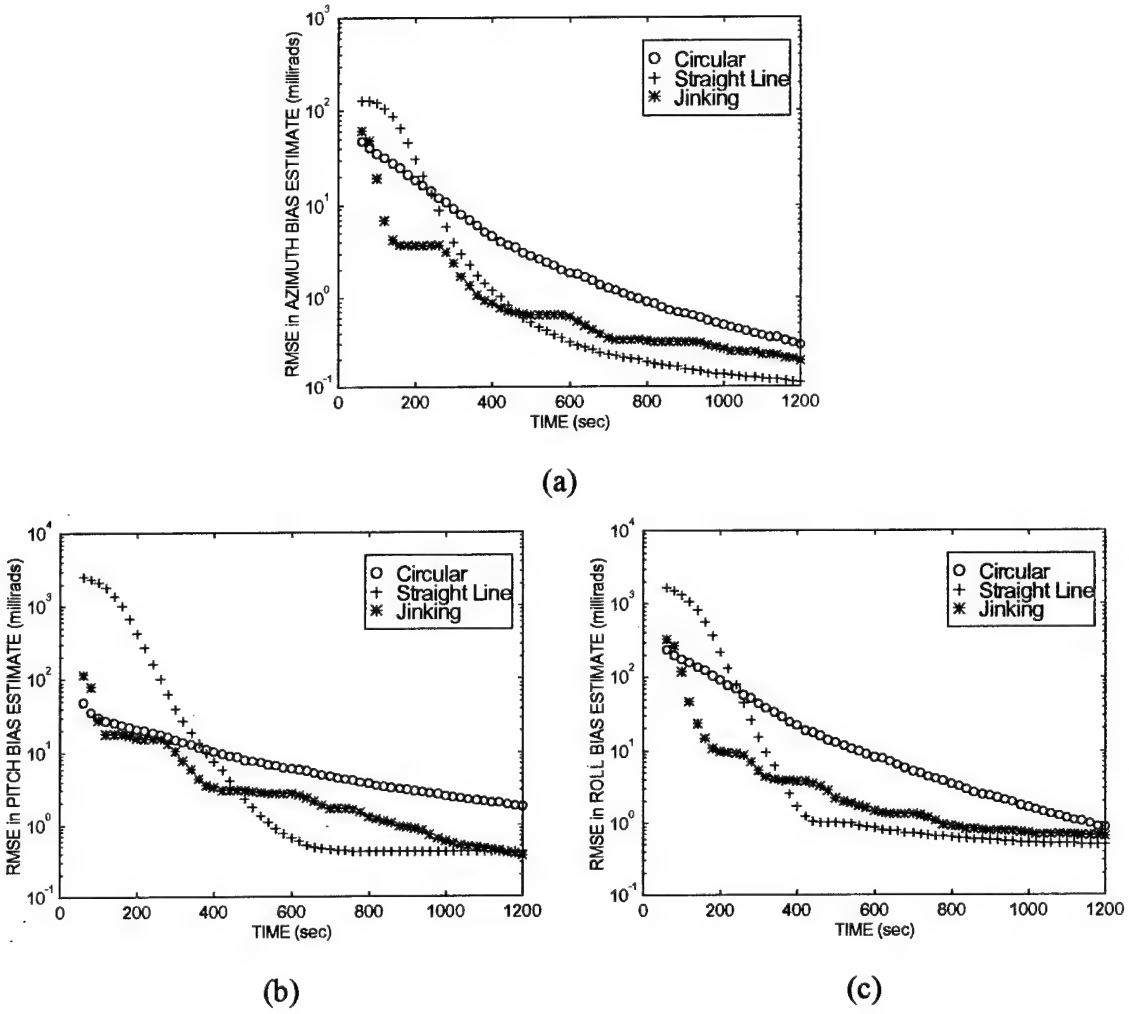

FIGURE 4-13. RMSEs IN THE ESTIMATES OF THE ANGULAR BIASES FOR A SENSOR ONLY MEASURING RANGE AND BEARING FOR THE STATIC ATTITUDE CASE: (a) AZIMUTH, (b) PITCH, AND (c) ROLL BIASES

The bias estimates were input to the bias correction module to remove the biases from the stabilized measurements reported by the sensor for the parabolic trajectory. The results are presented in Figure 4-14. The unaligned and aligned RMSEs for the range are presented in (a), and the unaligned and aligned RMSEs for the bearing in (b). The circles are the aligned RMSEs for the circular trajectory, the plus-marks are the aligned RMSEs for the straight line trajectory, the stars are the aligned RMSEs for the jinking trajectory, the solid lines are the unaligned RMSEs in the stabilized coordinates, and the dashed lines represent the values of the standard deviations in the stabilized coordinates due only to the random error.

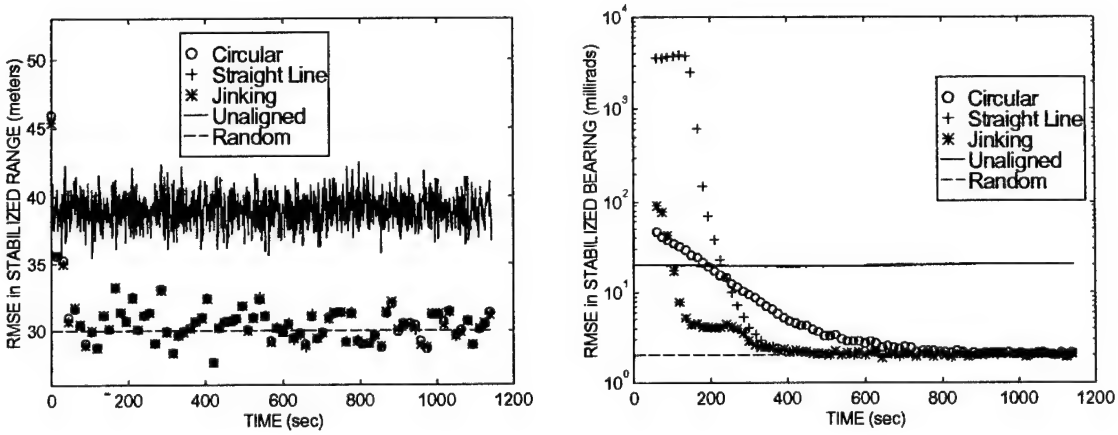

(a) (b)

FIGURE 4-14. UNALIGNED AND ALIGNED ERRORS IN THE PARABOLIC TRAJECTORY FOR A SENSOR ONLY MEASURING RANGE AND BEARING FOR THE STATIC ATTITUDE CASE: (a) RANGE AND (b) BEARING

The results for the stabilized range are very similar to the results obtained for the sensor measuring range, bearing, and elevation. For the stabilized bearing, the errors in the aligned

bearing are initially much larger than for the unaligned bearing; that is, the performance is initially degraded by correcting the stabilized bearing. This occurs for all three trajectories that were used to estimate the biases. It takes about 400 s for the straight line and jinking trajectories to produce an accurate alignment for the stabilized bearing, and about 700 s for the circular trajectory. Thus, it takes considerably longer to accurately align the stabilized bearing compared to the sensor measuring range, bearing, and elevation (see Figure 4-5(b)).

4.4 DISCUSSION

The range bias is easily estimated using any of the three trajectories considered in the bias estimation module. The accuracy and convergence of the range bias estimates were nearly identical for any of the trajectories and nearly the same for both the static and dynamic attitude cases. Also, the results were nearly identical for the sensor measuring range, bearing, and elevation, and the sensor only measuring range and bearing.

The accuracy and convergence of the angular biases estimates do depend on the trajectory used in the bias estimation module, the attitude of the sensor, and the type of sensor. The estimates of the angular biases were more accurate and converged more quickly for the sensor measuring range, bearing, and elevation (and, thus, also for a sensor only measuring bearing and elevation) than for the sensor only measuring range and bearing (and, thus, also for a sensor only measuring bearing). The decrease in accuracy and the longer convergence times for a sensor only measuring range and bearing occurred because there was only one measurement equation for the angular biases (i.e., Equation (3-65)) whereas the sensor measuring range, bearing, and elevation had two measurement equations for the angular biases (i.e., Equations (3-65) and (3-66)).

After the initial errors in the bias estimates subsided, the straight line trajectory usually produced the most accurate estimates of the angular biases. This was probably due to the larger bearing displacements between successive points on the straight line trajectory as it neared the sensor. Conversely, during the initial part of the straight line trajectory, the bearing displacements were smaller than for the circular and jinking trajectories, and this was manifested by larger initial estimation errors in the biases for the straight line trajectory. Thus, it appears that to obtain accurate bias estimates that also converge quickly, the trajectory used in the bias estimation module should have the largest possible bearing displacements between successive points on the trajectory. These bearing displacements are mainly influenced by the shape of the trajectory, by the distance of the trajectory from the sensor, and by the target speed. Future work needs to be conducted in determining the factors (e.g., trajectory shape, distance from the sensor, target speed, etc.) that improve the accuracies of the bias estimates. As an alternative, one could use two or more targets simultaneously in the bias estimation module to attempt to improve the accuracies of the estimates.

Once the biases were estimated, they were used in the bias correction module to align the stabilized coordinates of the parabolic trajectory. The alignment of the stabilized range was always very good. After the initial errors in the biases subsided, the alignments of the stabilized bearing and stabilized elevation were also fairly good. The only exceptions were the slight increases in the error for the aligned elevation between 400 and 800 s when the circular or jinking trajectories were used to estimate the biases. This was due to the estimation error in the biases and the shape of the parabolic trajectory. This problem was less noticeable for the straight line trajectory because the estimates of the biases are more accurate for the straight line trajectory in this time interval. For the sensor measuring range, bearing, and elevation (and for a sensor only measuring bearing and elevation), it took about 200 s to accurately align the bearing and elevation. However, because of the increased errors in the estimates of the angular biases, it takes about 400

to 600 s to accurately align the bearing for the sensor only measuring range and bearing (and for a sensor only measuring bearing).

A study was also conducted to determine the effects of the accuracy of the absolute standard on the alignment. Absolute standards with total positional accuracies of 1 m, 30 m, and 100 m were simulated. As expected, the accuracies of the bias estimates were best for the 1 m standard, followed by the 30 m standard, and then by the 100 m standard. The accuracies in the range bias estimates for the 30 m standard were about 20% larger than for the 1 m standard, and the accuracies in the estimates of the angular biases were about 50% larger than for the 1 m standard. For the 100 m standard, the accuracies in the range bias estimates were about 130% larger than for the 1 m standard, and the accuracies in the estimates of the angular biases were about 300% larger than for the 1 m standard. In removing the bias errors from the stabilized coordinates of the parabolic trajectory, the results for the three standards were surprisingly similar after the initial errors in the bias estimates subsided. Of course, the 1 m standard provided the best overall performance. However, the 30 m standard gave about 98% of the average alignment performance of the 1 m standard in removing the biases from the stabilized measurements of the parabolic trajectory. The 100 m standard gave 99% of the average alignment performance of the 1 m standard in removing the biases from the stabilized bearing, and about 85% of the performance of the 1 m standard in removing the biases from the stabilized range and the stabilized elevation. These numbers were obtained by averaging the RMSEs for the parabolic trajectory from 200 to 1142 s. Thus, in removing the biases from the stabilized coordinates of the parabolic trajectory, only marginal gains were realized in going from a 30 m standard to a 1 m standard. Larger gains were obtained in going from a 100 m standard to either a 30 m or a 1 m standard. Of course, these numbers are averages over a time interval and apply only to the parabolic trajectory. The same conclusions may not hold for other trajectories or at any particular instant of time.

5.0 SUMMARY

The absolute alignment problem was examined in this report. An algorithm was developed for absolutely aligning the positional data reported by a tracking sensor using a target whose location is measured by the sensor and whose location can also be precisely determined by some technique independently of the sensor's measurements. This algorithm also required the location of the sensor to be precisely known. Any differences between the sensor-reported position for the target and its independently determined precise location were attributed to bias errors in the positional data reported by the sensor. These differences were then used to estimate the bias errors in the positional data reported by the sensor. A potential candidate for providing precise location information independently of the sensor's measurements is GPS. However, the algorithm is applicable to any technique that provides precise location information independently of the sensor's measurements.

The absolute alignment algorithm consisted of two basic modules: (1) the bias estimation module, and (2) the bias correction module. The bias estimation module was used to estimate the bias errors using the difference between a target's sensor-reported position and its independently determined precise location. Two decoupled filters were used in the bias estimation module to estimate the biases: a filter to estimate the range bias and another one to estimate the angular biases. The bias correction module received estimates of the biases from the bias estimation module and then used these estimates to remove the biases from the sensor-reported positional data. Note that the bias correction module corrects the positional data for all of the targets reported by the sensor, not only the target used to estimate the biases.

Simulations were used to illustrate the performances of the absolute alignment algorithms for the four most common types of tracking sensors providing positional data. Various trajectories were used in the bias estimation module to determine the effects of a trajectory in estimating the biases. Specifically, circular, straight line, and jinking trajectories were used in the bias estimation module. The range bias was easily estimated using any of the trajectories. The accuracy and convergence of the range bias estimate were nearly identical for any of the trajectories. However, the accuracy and convergence of the angular biases estimates did depend on the trajectory and the type of sensor reporting the positional data. The estimates of the angular biases were more accurate and converged more quickly for the sensor measuring range, bearing, and elevation (and, thus, also for a sensor only measuring bearing and elevation) than for the sensor only measuring range and bearing (and, thus, also for a sensor only measuring bearing). The decrease in accuracy and the longer convergence times for a sensor only measuring range and bearing occurred because there was only one measurement equation for the angular biases whereas the sensor measuring range, bearing, and elevation had two measurement equations for the angular biases.

After the initial errors in the bias estimates subsided, the straight line trajectory usually produced the most accurate estimates of the angular biases. This was probably due to the larger bearing displacements between successive points on the straight line trajectory as it neared the sensor. Conversely, during the initial part of the straight line trajectory, the bearing displacements were smaller than for the circular and jinking trajectories, and this was manifested by larger initial estimation errors in the biases for the straight line trajectory. Thus, it appears that to obtain accurate bias estimates that also converge quickly, the trajectory used in the bias estimation module should have the largest possible bearing displacements between successive points on the trajectory. These displacements are mainly influenced by the shape of the trajectory, by the distance of the trajectory from the sensor, and by the target speed. Future work needs to be conducted in determining the factors (e.g., trajectory shape, distance from the sensor, target speed, etc.) that improve the accuracies of the bias estimates.

The bias estimates were input to the bias correction module to align the stabilized measurements reported by the sensor. A trajectory which was different from any of those used to estimate the biases was used in the bias correction module. This was done to determine how well the biases could be removed from a track's measurements when a different track was used to generate the bias estimates. Specifically, a target with an approximate parabolic trajectory was used in the bias correction module. The alignment of the stabilized range was always very good. After the initial bias errors subsided, the alignments of the stabilized bearing and the stabilized elevation were also good. For the sensor measuring range, bearing, and elevation (and a sensor only measuring bearing and elevation) it took about 200 s (i.e., 200 data points) before the bearing and elevation were accurately aligned. However, for the sensor only measuring range and bearing (and a sensor only measuring bearing), it took about 400 to 600 s (i.e., 400 to 600 data points) to accurately align the bearing. This was due to the larger estimation errors in the angular biases for the sensor only measuring range and bearing.

A study was also conducted to determine the effects of the accuracy of the absolute standard on the alignment. Absolute standards with total positional accuracies of 1 m, 30 m, and 100 m were simulated. As expected, the accuracies of the bias estimates were best for the 1 m standard, followed by the 30 m standard, and then by the 100 m standard. The accuracies in the range bias estimates for the 30 m standard were about 20% larger than for the 1 m standard, and the accuracies in the estimates of the angular biases were about 50% larger than for the 1 m standard. For the 100 m standard, the accuracies in the range bias estimates were about 130% larger than for the 1 m standard, and the accuracies in the estimates of the angular biases were about 300% larger than for the 1 m standard. In removing the bias errors from the stabilized coordinates of the parabolic trajectory, the results for the three standards were surprisingly similar after the initial errors in the bias estimates subsided. Of course, the 1 m standard provided the best overall performance. However, the 30 m standard gave about 98% of the average alignment performance of the 1 m

standard in removing the biases from the stabilized measurements of the parabolic trajectory. The 100 m standard gave 99% of the average alignment performance of the 1 m standard in removing biases from the stabilized bearing, and about 85% of the performance of the 1 m standard in removing the biases from the stabilized range and the stabilized elevation. Thus, in removing the biases from the stabilized coordinates of the parabolic trajectory, only marginal gains were realized in going from a 30 m standard to a 1 m standard. Larger gains were obtained in going from a 100 m standard to either a 30 m or 1 m standard. Of course, these numbers are averages over a time interval and apply only to the parabolic trajectory. The same conclusions may not hold for other trajectories or at any particular instant of time.

Finally, the algorithms developed in this report can also be applied to the relative alignment problem provided that there are no bias errors in the locations of the sensors and that the master sensor is a sensor measuring range, bearing, and elevation. In this case, the master sensor measuring range, bearing, and elevation would play the role of the absolute standard in the algorithms developed in this report. The resulting relative alignment algorithms will be more general than the ones developed by Helmick *et al.*,[4-7] and thus supersedes them. For example, they assumed that the bias errors were small and that the pitch, roll, and yaw angles were also small. None of these assumptions were used to develop the general nonlinear algorithm presented in this report. Of course, the linear algorithm presented in this report did assume that the angular biases were small. Also, they assumed that the distances between the sensors were small (i.e., co-located). This would not be a limitation in the new relative alignment algorithms because the alignment would be performed in the stabilized frame of the sensor to be relatively aligned. In this case, the data reported by the master sensor would be transformed to the other sensor's stabilized frame and this leads to our requirements that the master sensor provide full three dimensional information for the position and that there be no bias errors in the locations of the sensors. Thus, the new relative alignment algorithms would also apply to widely separated sensors

REFERENCES

1. Conte, J. E., and Helmick, R. E., "Real-Time Bias Estimation and Alignment of Two Asynchronous Sensors for Track Association and Fusion," Naval Surface Warfare Center Dahlgren Division, NSWCDD/TR-94/285, April 1995.

2. Frieden, D. R., ed., *Principles of Naval Weapons Systems*, Naval Institute Press: Annapolis, MD, 1985.

3. Goldstein, H. L., *Classical Mechanics*, Addison-Wesley: Reading, MA, 1980.

4. Helmick, R. E., and Rice, T. R., "Removal of Alignment Errors in an Integrated System of Two 3-D Sensors," *IEEE Transactions on Aerospace and Electronic Systems*, vol. 29, no. 4, October 1993.

5. Helmick, R. E., and Rice, T. R., "Registration of a 3D Sensor and a 2D Sensor Measuring Range and Azimuth," in *Proc. of Signal and Data Processing of Small Targets 1993*, SPIE Orlando '93, vol. 1954, Orlando, FL, April 1993.

6. Helmick, R. E., and Rice, T. R., "Alignment of a 2D Sensor and a 3D Radar," in *Proc. of Acquisition, Tracking, and Pointing VI*, SPIE Orlando '92, vol. 1697, Orlando, FL, April 1992.

REFERENCES (continued)

7. Helmick, R. E., and Rice, T. R., "Alignment of a 3-D Sensor and a 2-D Sensor Measuring Azimuth and Elevation," Naval Surface Warfare Center Dahlgren Division, NSWCDD/TR-92/181, April 1992.

8. Bar-Shalom, Y., and Li, X. R., *Estimation and Tracking: Principles, Techniques, and Software*, Artech House: Boston, 1993.

9. Gelb, A., ed., *Applied Optimal Estimation*, The M.I.T. Press: Cambridge, MA, 1974.

DISTRIBUTION

	COPIES
DOD ACTIVITIES (CONUS)	
ATTN D VAUGHN AWT DIRECTORATE MARINE CORPS SYSTEMS COMMAND 2033 BARNETT AVENUE QUANTICO VA 22134-5010	1
ATTN DR RABINDER MADAN 1114SE CHIEF OF NAVAL RESEARCH BALLSTON TOWER 1 800 N QUINCY ST ARLINGTON VA 22217-5660	1
ATTN A76 (TECHNICAL LIBRARY) COMMANDING OFFICER CSSDD NSWC 6703 W HIGHWAY 98 PANAMA CITY FL 32407-7001	1
DEFENSE TECHNICAL INFORMATION CTR 8725 JOHN J KINGMAN RD SUITE 0944 FT BELVOIR VA 22060-6218	2
NON-DOD ACTIVITIES (CONUS)	
ATTN DR FRANK RIEFLER GOVERNMENT ELECTRONIC SYSTEMS DIVISION LOCKHEED MARTIN CORP MOORESTOWN NJ 08057	1
ATTN PROF YAAKOV BAR SHALOM ESE DEPARTMENT U 157 260 GLENBROOK RD STORRS CT 06269-3157	1
ATTN DR A T ALOUANI DEPT OF ELECTRICAL ENGINEERING TENNESSEE TECHNOLOGICAL UNIV TTU BOX 05004 COOKEVILLE TN 38505	1
ATTN PROF R H BISHOP DEPT OF AEROSPACE ENGINEERING AND ENGINEERING MECHANICS THE UNIV OF TEXAS AT AUSTIN AUSTIN TX 78712	1
ATTN DR OLIVER E DRUMMOND INDEPENDENT CONSULTING ENGINEER 10705 CRANKS ROAD CULVER CITY CA 90230	1
ATTN DR SAM BLACKMAN HUGHES AIRCRAFT COMPANY BLDG E01 MS A173 PO BOX 902 EL SEGUNDO CA 90245	1
ATTN MELVIN L BELCHER JR MANAGER MISSILE DEFENSE RADAR SYSTEMS GEORGIA TECH RESEARCH INSTITUTE GEORGIA INSTITUTE OF TECHNOLOGY SENSORS AND ELECTROMAGNETIC APPLICATIONS LABORATORY RADAR SYSTEMS DIVISION ATLANTA GA 30332-0800	1
THE CNA CORPORATION PO BOX 16268 ALEXANDRIA VA 22302-0268	1

DISTRIBUTION (Continued)

	COPIES
ATTN EDWARD PRICE UNITED DEFENSE 1 DANUBE DR KING GEORGE VA 22485	1
ATTN GIFT AND EXCHANGE DIV LIBRARY OF CONGRESS WASHINGTON DC 20540	4

INTERNAL

B		1
B30		1
B32		1
B32	(BLAIR)	1
B32	(CONTE)	20
B32	(GENTRY)	1
B32	(GROVES)	1
B32	(HELMICK)	20
B32	(RICE)	20
B32	(WATSON)	1
B35	(BAILEY)	1
B35	(FENNEMORE)	1
B35	(HARTER)	1
B60	(TECHNICAL LIBRARY)	1
G23	(OHLMEYER)	1
G305	(STIEGLER)	1
N24	(BOYER)	1
N24	(MURRAY)	1
N24	(SERAKOS)	1
T43	(GRAY)	1